

Electrically driven structures in bent-core nematics

Nándor Éber^a, Ágnes Buka^a and K. S. Krishnamurthy^b

^aInstitute for Solid State Physics and Optics, Wigner Research Centre for Physics, Eötvös Loránd Research Network, Budapest, Hungary; ^b Centre for Nano and Soft Matter Sciences, Survey No. 7, Shivanapura, Bangalore 562162, India.

Corresponding author: Nándor Éber, Institute for Solid State Physics and Optics, Wigner Research Centre for Physics, Eötvös Loránd Research Network, 1525 Budapest, P. O. Box 49, Hungary, e-mail: eber.nandor@wigner.hu

Provide short biographical notes on all contributors here if the journal requires them.

Electrically driven structures in bent-core nematics

This review, dedicated to the memory of B. K. Sadashiva, concerns electrically driven patterns and defects in bent core nematics (BCNs) made of hard-core, soft-core or bent-rod type of molecules. It covers (a) spatially periodic patterns associated with electroconvection and flexoelectric deformation, (b) dislocations in these patterned states and (c) various types of defects induced essentially in homogeneous, unpatterned states of BCNs. While in general, the wealth of pattern morphologies is just as rich in BCNs as in rod-like nematics, certain features of electroconvection have so far been observed only in some BCN materials. Some attributes relating to the generation and behaviour of defects in electric field may also be ascribed to material properties specific to BCNs. It is also shown that the electric field induced patterns as well as their modification by light irradiation may serve as optical gratings and thus establishes the background for designing new photonic devices.

Keywords: bent-core nematics; electroconvection; flexoelectric domains; topological defects; optical gratings

Subject classification codes: include these here if the journal requires them

1. Introduction

For many decades, it was largely believed that liquid crystallinity mostly requires a rod- or disc-like shape of the constituting molecules. This situation has changed during the last 25 years upon the discovery of exciting new forms of mesomorphism in banana-shaped (bent-core, BC) compounds. The field of BC liquid crystals has come to be widely recognized due to the seminal contributions of, among others, B. K. Sadashiva in whose memory and honour this review series is being brought out. His work in the period 1998-2019 on the syntheses of novel BC molecules and physical characterization of their mesophases has significantly advanced the field. We note that his work includes a study of electroconvection in BC nematics, which is, in part, a subject of this review.

BC materials have been found to exhibit numerous novel mesophases [1, 2, 3], among them those allowing the occurrence of ferroelectricity and polar switching in a system composed of achiral molecules [4]. Many BC compounds possess exotic, low-symmetry and/or polar smectic phases; nevertheless, some BC materials exhibit a nematic phase as well.

While characteristics of BC nematics (BCNs) resemble those of conventional (rod-like or calamitic) nematics in many aspects, some investigations have also explored unusual behaviour, which have recently been discussed in comprehensive reviews [3, 5, 6, 7]. The specialities of BCN materials, for example, include unusually high viscosities [8], $\frac{K_3}{K_1} < 1$ elastic constant ratios [9, 10, 11], dielectric relaxation at exceptionally low frequencies of a few kHz [12, 13] and giant flexoelectricity, i.e., a bend flexoelectric constant $e_3 \sim 10 \text{ nC cm}^{-2}$, exceeding by three orders of magnitude that of calamitic nematics [14].

The nanostructure of the nematic phase of BCNs may also exhibit significant distinction compared to that of calamitic nematics. Due to their bent molecular structure, some BCN molecules tend to form a local polar order in the form of dynamic smectic clusters. The existence of such smectic clusters was first suggested to interpret light scattering and NMR measurements and was later justified by X-ray diffraction and transmission electron-microscopy of freeze fractured samples [15, 16, 17, 18, 19]. We note that cybotactic clusters may also exist in calamitic nematics, however, only as a pretransitional effect in the near vicinity of phase transitions. In contrast, the smectic clusters exist in the nematic phase of certain BCNs in the whole nematic range, prevailing for several degrees also in their isotropic phase; therefore, the nematic phase of such BCNs is also known as a cybotactic nematic phase.

A rather controversial issue has arisen related to the symmetry of the nematic phase of BCNs. One important property of the common nematic phase is its uniaxial symmetry. Theoretical considerations implied that a nematic phase with a biaxial symmetry might also exist [20]; however, so far, it has been experimentally observed only in a lyotropic material [21]. In search for a thermotropic biaxial nematic phase, BCNs are natural candidates, as BCN molecules have a biaxial character. Indeed, several BCN molecules have been claimed to possess a biaxial nematic phase; however, for each observation an alternative explanation assuming uniaxial symmetry could also be given [3].

While the existence of a biaxial thermotropic nematic phase could not be justified yet, discovery of another type of nematic, the twist-bend nematic (N_{TB}) phase has firm theoretical [22] and experimental proofs [23, 24].

BC nematics, just as the rod-like ones, interact with an electric field. Depending on the cell geometry and the electric anisotropies, the electric field induced director distortions are either spatially homogeneous (such effects are utilized in LC displays) or inhomogeneous, forming patterns. Some patterns are spatially periodic, composed of a sequence of repetitive units. Others, commonly known as defects, rather represent some discontinuity in the director field.

In the present review, we focus on various patterns induced by an electric field in BCNs. First, in Section 2, we survey the BC nematics reported to exhibit such phenomena. Then, Section 3 is devoted to the two main mechanisms resulting in periodic patterns, electroconvection and flexoelectric domains. Finally, in Section 4 different aspects of defects and their interaction with electric field are addressed.

2. Materials

Though by now numerous BCN compounds have been synthesized, the majority of

them has either not been tested for the patterns or not revealed any patterned state. The compounds for which the existence of patterns have been reported, can be grouped into three families: (a) hard-core BCNs, HBCN1-HBCN17 (see Figure 1 and Table 1), in which the rigid core determines the opening angle of the arms; (b) soft-core BCNs, SBCN1-SBCN5 (see Figure 2 and Table 2), which are actually dimers of rod-like units connected by an odd-number-length flexible chain, capable to form a twist-bend nematic phase; and (c) dimers DBCN1-DBCN4 (see Figure 3 and Table 3) composed of rod-like and BCN units, connected by a flexible chain.

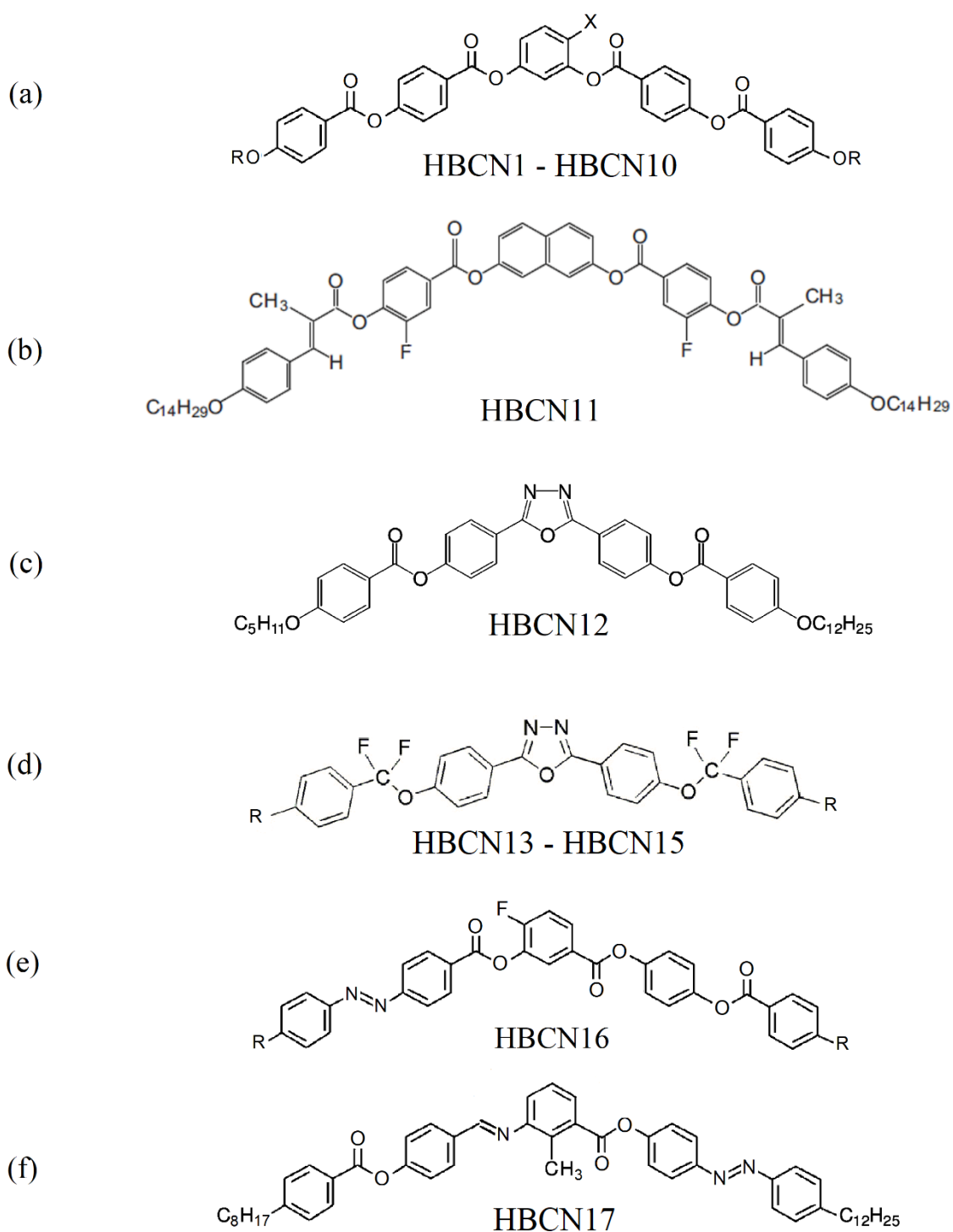


Figure 1. Structural formulas of hard-core BCN compounds.

Table 1. List of hard-core BCN compounds with reported occurrence of patterns.

Code name	Structural formula	X	R	Original code name	References
HBCN1	Figure 1(a)	Cl	-O(CH ₂) ₆ CH=CH ₂	ClPbis10BB	[25, 26, 27, 28, 29, 30]

HBCN2	Figure 1(a)	Cl	-OC ₉ H ₁₉	9Cl	[31]
HBCN3	Figure 1(a)	Cl	-OC ₁₀ H ₂₁	M1118	[32]
HBCN4	Figure 1(a)	Cl	-OC ₁₁ H ₂₃	11Cl	[33, 34, 35]
HBCN5	Figure 1(a)	Cl	-OC ₁₂ H ₂₅	12Cl	[36]
HBCN6	Figure 1(a)	Br	-OC ₁₂ H ₂₅	12Br	[31]
HBCN7	Figure 1(a)	CN	-OC ₆ H ₁₃	6OCN	[37]
HBCN8	Figure 1(a)	CN	-OC ₈ H ₁₇	1c	[38]
HBCN9	Figure 1(a)	CN	-OC ₉ H ₁₉	9OCN	[13, 39]
HBCN10	Figure 1(a)	CN	-OC ₁₂ H ₂₅	CNRbis12OBB	[40]
HBCN11	Figure 1(b)	-	-	-	[41]
HBCN12	Figure 1(c)	-	--	C5-Ph-ODBP- Ph-OC12	[42, 43, 44]
HBCN13	Figure 1(d)	-	-C ₇ H ₁₅	7P-CF ₂ O- ODBP	[45, 46, 47, 48, 49, 50]
HBCN14	Figure 1(d)	-	-C ₈ H ₁₇	8P-CF ₂ O- ODBP	[51, 48]
HBCN15	Figure 1(d)	-	-C ₉ H ₁₉	9P-CF ₂ O- ODBP	[52, 48]
HBCN16	Figure 1(e)	-	-	SV775	[53]
HBCN17	Figure 1(f)	-	-	A131	[54]

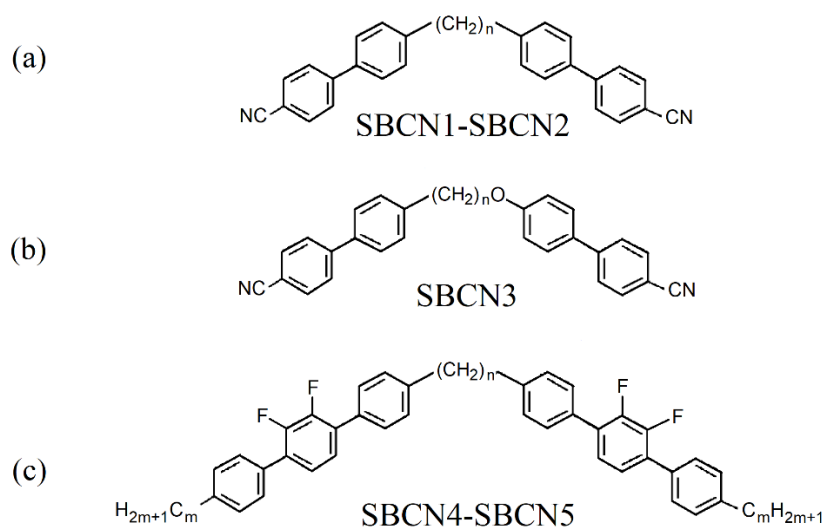


Figure 2. Structural formulas of soft-core BCN compounds.

Table 2. List of soft-core BCN compounds with reported occurrence of patterns.

Code name	Structural formula	n	m	Original code name	References
SBCN1	Figure 2(a)	7	-	CB7CB	[55, 56, 57, 58, 59, 60]
SBCN2	Figure 2(a)	11	-	CB11CB	[61, 62, 63]
SBCN3	Figure 2(b)	6	-	CB6OCB	[64]
SBCN4	Figure 2(c)	11	3	M2	[61, 65, 66, 62]
SBCN5	Figure 2(c)	11	5	M3	[61, 62]

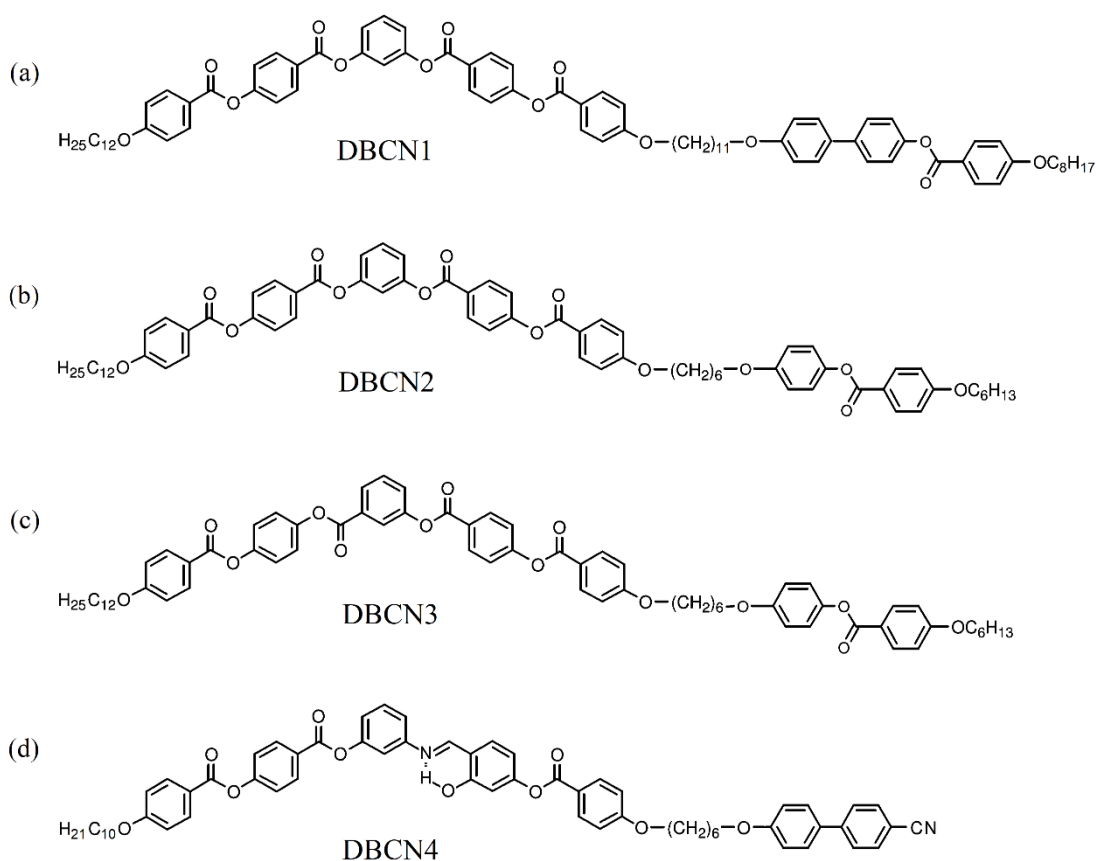


Figure 3. Structural formulas of dimers with rod-like and bent-core units.

Table 3. List of dimers with rod-like and bent-core units, with reported occurrence of patterns.

Code name	Structural formula	Original code name	References
DBCN1	Figure 3(a)	1a	[67]
DBCN2	Figure 3(b)	1b	[67]
DBCN3	Figure 3(c)	GPT 340	[68, 69, 70, 71]
DBCN4	Figure 3(d)	BCCB	[72, 73]

3. Periodic patterns

Studies on calamitic nematics have pointed out that the two main kinds of pattern-forming mechanisms active in these compounds under excitation by an electric field are electroconvection (EC) and flexoelectric distortions [74].

EC has mostly been observed upon application of an ac voltage exceeding a frequency dependent threshold value $U_c(f)$ with f being in the audio frequency range. In EC, the director modulation that results in periodic stripes with visible colour and/or intensity contrast in a polarising microscope, is accompanied with material and charge flows; thus a finite electrical conductivity is vital for the occurrence of EC. The patterns can be classified into standard EC (s-EC) and nonstandard EC (ns-EC) [75], depending on whether the continuum description of EC (the so-called standard model, SM [76]) provides an explanation for the pattern formation or does not. Within both EC types, different pattern morphologies, i.e., various directions of the wave vector \mathbf{q} of the pattern with respect to the initial director \mathbf{n}_0 (the rubbing direction of planar samples) can be observed by varying the frequency and voltage [75, 74]. These include normal rolls (NR, $\mathbf{q} \parallel \mathbf{n}_0$), longitudinal rolls (LR, $\mathbf{q} \perp \mathbf{n}_0$) and oblique rolls (OR) with an obliqueness angle $0^\circ < \alpha < 90^\circ$. For the majority of patterns the convection within the rolls occurs in a plane perpendicular to the substrates, as proven by observing the motion of added foreign particles. There exist, however, patterns with in-plane convection parallel with the substrates. Their most common example is the prewavy (PW) pattern [77], which corresponds to in-plane normal rolls (INR); while, as we will see later, in BCNs in-plane longitudinal rolls (ILR) have also been observed.

Experimental and theoretical studies have concluded that the nature of EC occurring in a given nematic depends mainly (but not exclusively) on the signs of the anisotropies of the dielectric permittivity (ϵ_a) and the electrical conductivity (σ_a). Therefore, it is convenient to divide nematics into four groups according to the possible combinations of (sign of ϵ_a , sign of σ_a) [75]. Compounds with different signs of the anisotropies, $(-, +)$ and $(+, -)$, are expected to exhibit standard EC, while those with identical signs, $(-, -)$ or $(+, +)$, facilitate typically nonstandard EC.

In contrast to EC, flexoelectricity induced distortions, the flexoelectric domains (FDs), mostly are observable at dc and at very low frequency ($f < 5$ Hz) ac voltages. FDs are not accompanied with flow and are observable only if the electrical conductivity is quite low (otherwise EC may take over). The signs of the anisotropies ϵ_a and σ_a play only a marginal role; nevertheless, some material parameters (ϵ_a , the flexoelectric coefficients, elastic moduli) of the nematic should fulfil certain constraint to allow the occurrence of FDs [78]. For these reasons, in general, reports on FDs are much scarcer than those on EC patterns.

In bent-core nematics, both of the above mentioned pattern forming mechanisms are also available. First mentionings of patterns in BCNs were byproducts of polarising microscopic characterisation of newly synthesized compounds HBCN2 [31], HBCN5 [36], HBCN6 [31], HBCN8 [38], DBCN1 [67], DBCN2 [67], HBCN17 [54] and SBCN2 [63]. Though the pattern types cannot be unambiguously identified merely based on the short descriptions and photos published, most probably HBCN2, HBCN5, HBCN8, DBCN1 and DBCN2 exhibited FD at dc field, while in DBCN1 longitudinal ns-EC rolls, in HBCN6 and HBCN17 another kind of ns-EC, the prewavy pattern [77] (also known as broad domains), in the common nematic phase of SBCN2 oblique EC rolls might have been observed. Later, detailed studies of pattern formation have been performed on several BCN compounds, which we review in the following, summarizing the similarities and dissimilarities with the behaviour of calamitic nematics. It has to be kept in mind, however, that such comparison is hindered by the fact that the material parameters of most BCN compounds have not been measured yet; occasionally, even the categorisation of materials by the anisotropy signs becomes problematic.

We note at this point that the twist-bend nematic (N_{TB}) phase of soft-core BCNs deserves a special attention, as periodic structures may occur in N_{TB} at multiple levels

[79]. First, there is a heliconical structure with a pitch of a few nanometers [23, 24]. Second, in planar cells there may exist a spontaneous periodic stripe pattern parallel with \mathbf{n}_0 , occurring even in the absence of an electric field, as found in SBCN1 [58], SBCN3 [64], SBCN4 [66], as well as SBCN5 [61]. This pattern is sensitive to the surface anchoring conditions [64]; it can be suppressed by a large magnetic field and was proposed to be a manifestation of a Helfrich-Hurault-type mechanism [80]. Transformation of the spontaneously periodic N_{TB} state of a dimeric mixture into the homeotropic state under the influence of a 1 Hz triangular wave field (upto 16 V/ μm) was also reported, attributed to defect mediated rotation of pseudolayers, similar to layer realignments in SmA and SmC* phases [81].

A sub-micrometer scale superstructure could also be detected by confocal microscopy [62]. In addition, excited by high ac electric field, a stripe structure composed of domains of opposite chirality (manifesting a spontaneous chiral symmetry breaking) develops, where the domains exhibit a fast, polar electro-optical switching [65, 62]. Recently the N_{TB} phase with its spontaneous periodic pattern has also been observed in an asymmetrical hard-core BCN too [82].

3.1. Electroconvection in BCNs

The first systematic studies of EC in BCNs were performed on HBCN1 [25, 26, 29]. HBCN1 is an excellent paradigm of bent-core nematics, as it has been investigated by numerous experimental methods and almost all of the distinctive features of BCNs mentioned in the Introduction have been detected in this compound [26]. EC in HBCN1 has been studied in a wide frequency range from 1 Hz to 100 kHz, which can be subdivided into four regions concerning the morphology of patterns (Figure 4).

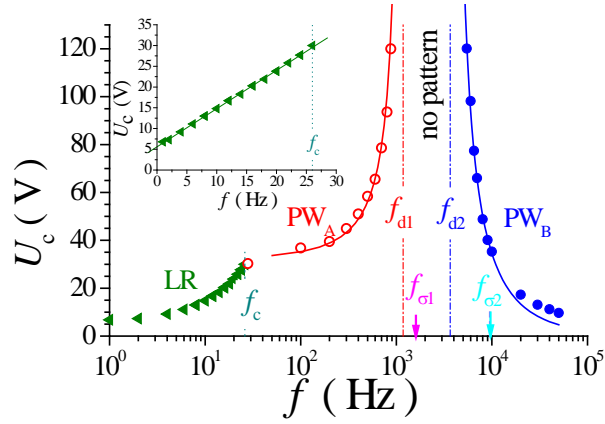


Figure 4. Frequency dependence of the threshold voltage $U_c(f)$ on a logarithmic frequency scale. The dotted line indicates the crossover frequency from longitudinal rolls (LR) to the lower f prewavy pattern (PW_A). The dash-dotted lines correspond to the divergence frequencies f_{d1} and f_{d2} of the lower (PW_A) and the higher f (PW_B) prewavy pattern, respectively. The arrows denote the sign inversion frequencies $f_{\sigma1}$ and $f_{\sigma2}$ of the electrical conductivity. The insert exhibits $U_c(f)$ of the LR range on a linear f scale. (After [25])

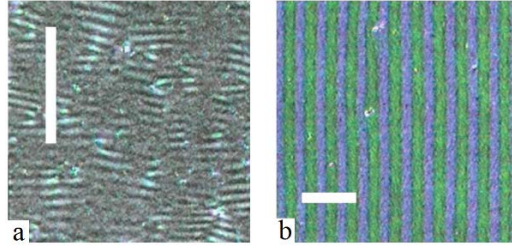


Figure 5. Snapshots of EC patterns in HBCN1. (a) Longitudinal rolls at $f = 12$ Hz and $U = 28$ V, (b) PW_A at $f = 200$ Hz and $U = 48$ V. The scale bars are $100 \mu\text{m}$ long, $d = 15 \mu\text{m}$. The rubbing direction \mathbf{n}_0 is horizontal, the crossed polars make an angle of 15° with \mathbf{n}_0 . (After [25])

At the lowest frequencies, for $f < f_c \approx 26$ Hz, longitudinal rolls (LR) running parallel to \mathbf{n}_0 and exhibiting a linear $U_c(f)$ threshold dependence were observed (Figure 5(a)). There exists an intermediate frequency range, $f_{d1} < f < f_{d2}$, where no pattern could be found. Below ($f_c < f < f_{d1}$) and above ($f_{d2} < f$) this pattern-free range, wide stripes perpendicular to \mathbf{n}_0 were detected, which were identified as a lower frequency PW_A and

a higher frequency PW_B versions of the prewavy pattern (Figure 5(b)). Interestingly, apart from their $U_c(f)$ behaviour, the PW_A and PW_B patterns are practically indistinguishable; their appearance and periodicity (being several times wider than the sample thickness d) are almost identical. The threshold voltage of PW_A diverges hyperbolically upon approaching f_{d1} from below: $U_c(f) \propto (f_{d1} - f)^{-1}$. A similar diverging threshold, $U_c(f) \propto (f - f_{d2})^{-1}$, was found for PW_B , just at approaching the frequency f_{d2} from above.

The scenarios shown in Figure 4 and outlined above are unprecedented among calamitic nematics in several aspects. First, in HBCN1, EC could be detected up to unusually high frequencies (100 kHz), while in calamitics the threshold voltage typically reaches the experimentally available limit already at a few kHz. Second, two distinct frequency ranges for the prewavy pattern have never been detected earlier. Third, the diverging threshold voltage of PW_A and PW_B is without precedence; former studies of the prewavy pattern indicated a smooth, nearly linear increase of $U_c(f)$. Fourth, in the PW_B range, $U_c(f)$ has a negative slope: $\frac{dU_c}{df} < 0$. In contrast to this, experiments on EC in calamitics have implied threshold voltages increasing with the frequency. Furthermore, theoretical models of EC developed so far also predict positive slope of $U_c(f)$. The only exception to this rule was found at very low, subhertz frequencies due to the artifact of internal voltage attenuation in measuring cells, caused by the resistance ratio of the aligning and the liquid crystal layers. As none of the above listed specialities have so far been identified in calamitic nematics, from now on we refer to them as ‘banana-specific’ features.

In an attempt to understand the behaviour above, one should focus on the frequency dependence of the signs of the anisotropies ϵ_a and σ_a . Dielectric measurements have shown that in HBCN1 $\epsilon_a < 0$ in the whole tested frequency range.

On the other hand, σ_a exhibited an unusual behaviour; it has changed its sign twice, at frequencies $f_{\sigma 1}$ and $f_{\sigma 2}$ [25]. Thus, at low ($f < f_{\sigma 1}$) and at high ($f > f_{\sigma 2}$) frequencies $\sigma_a < 0$, while in between ($f_{\sigma 1} < f < f_{\sigma 2}$) $\sigma_a > 0$. This behaviour is due to a low frequency dielectric relaxation present in the BCN. Comparing the sign inversion frequencies with the bounding frequencies of the morphological regions, one finds the sequence $f_c < f_{d1} < f_{\sigma 1} < f_{d2} < f_{\sigma 2}$ (see Figure 4).

As concluded from the dielectric measurements, HBCN1 belongs to the $(-, -)$ class at the lowest frequencies; therefore, LR is just the kind of morphology, which is expected for that class of materials. Interestingly, the threshold divergence of PW_A occurs at $f_{d1} < f_{\sigma 1}$, i.e., the whole PW_A range falls to that frequency domain, where the material is still of the $(-, -)$ class. In contrast to that, the second sign inversion frequency $f_{\sigma 2}$ is in the middle of the PW_B range, i.e., at its threshold divergence frequency f_{d2} the compound is part of the $(-, +)$ class, but becomes $(-, -)$ again at higher frequencies, where the threshold of PW_B diminishes. Unfortunately, the formation mechanism of the prewavy patterns and with that the reason for the threshold divergences are yet unexplored; nevertheless, the observations suggest that the sign of the conductivity anisotropy does not play an important role in PW formation and there is no direct correlation between the divergence and the sign inversion frequencies. Hence, the occurrence of the ‘banana-specific’ features still awaits an explanation.

As the EC scenarios found in HBCN1 are so much different from those observed in calamitic nematics, the effect of dilution of HBCN1 by the rod-like 6OO8 of the $(-, +)$ class was also studied [28]. At high (70 wt%) HBCN1 content, the ‘banana-specific’ features were still present, just the two divergence frequencies shifted toward higher f and at the lowest frequencies oblique or normal rolls of the conductive s-EC replaced the LR of ns-EC. At medium (50 wt%) HBCN1 content, the threshold curves still

exhibit similar frequency dependence; however, at high frequencies, instead of PW_B an aperiodic deformation was only visible. Finally, at low (30 wt%) HBCN1 content, the low f conductive rolls still turned into a PW pattern of steeply increasing threshold upon increasing f , but at high frequencies (above a few kHz) no patterns existed. Thus we can conclude that dilution by a calamitic nematic suppressed the ‘banana-specific’ properties of EC.

We note here that, though independent dielectric spectroscopic studies have been performed on the mixtures confirming the presence of a low f relaxation in a wide frequency range [12], unfortunately, no data were given on the frequency dependence of σ_a . The observation of s-EC patterns in the mixtures, however, imply that mixing with the calamitic might have cancelled the sign inversion of σ_a , i.e the mixtures belonged to the $(-,+)$ class in the whole relevant frequency range. This corroborates the suspicion that the sign of σ_a is not a relevant reason for the ‘banana-specificity’; rather the increased dielectric loss owing to the low f dielectric relaxation may play a role.

As an extension to the above studies, the influence of conductivity on the pattern morphologies has also been tested by doping the 70 wt% HBCN1 containing mixture with a 0.01–1 wt% conductive ionic salt [28]. It is well known from studies on calamitics that conductive s-EC rolls can occur only below a cut-off frequency, which is roughly proportional to the conductivity of the sample. This behaviour holds for the studied doped material too. The conductive s-EC—prewavy crossover frequency, f_c , shifted towards higher f upon doping; f_c of the highest doped mixture was two decades higher than that of the undoped one. As another effect of doping, the pattern-free frequency region disappeared; the divergences of the PW thresholds changed to a maximum, as if f_{d1} exchanged place with f_{d2} yielding a crossing of hyperboles. The location of the maximum moved to higher f , while its height diminished for stronger

doping; finally, at 1 wt% doping, only a flat PW threshold curve remained without a section with negative slope.

Based on these tests we can conclude that increasing the electrical conductivity weakens the ‘banana-specificity’. This observation, however, proves that the gradual disappearance of the ‘banana-specific’ properties of EC during dilution of HBCN1 by the rod-like 6OO8 described above is not related to the change of the conductivity of the mixture, since adding 6OO8 reduced the conductivity. The most significant change, the disappearance of the high f pattern with negative slope of $U_c(f)$, occurred reducing the BCN content below 50 wt%. Interestingly, other measurements on the HBCN1/6OO8 system explored that at around the same concentration range, significant changes occur in the dielectric relaxation [12], in the linear electromechanical response [83] as well as in the nanostructure (in the presence of cibotactic groups) [18].

HBCN1 is not the only material with ‘banana-specific’ properties; similar scenarios have been detected in HBCN11 and HBCN4 too. In HBCN11, both diverging prewavy patterns, the low f PW_A with positive and the high f PW_B with the negative slope of $U_c(f)$ are present [41]. However, the frequency gap between them was not completely pattern-free; an obscure prewavy pattern could be seen even in that range, while at the lowest frequencies, below the PW_A , instead of convection rolls a polydomain structure was visible. In contrast to the traditional assumption on PW pattern that the director has an alternating twist in the midplane of the cell, but not at the bounding plates [77], based on their polarising microscopic observations Tanaka et al. [41] proposed an alternating twisted-splayed structure for the PW, which involves surface pretilt and a net director rotation between the opposite surfaces. In addition, they reported that PW_B disappears at very high frequencies in a voltage-induced nematic-to-isotropic phase transition occurring due to heating by the dielectric loss. This raises the

possibility that a temperature change by dielectric heating may influence the behaviour already at lower frequencies and voltages as well.

Dielectric properties of HBCN4 are very similar to those of HBCN1, exhibiting a double sign inversion of σ_a [13]. At low f , it exhibits the longitudinal rolls of ns-EC expected in a (-,-) material. PW_A with positive and PW_B with the negative $U_c(f)$ slope (termed in-plane normal rolls INR2 and INR1, respectively in [13]) are both present, however, there is no full threshold divergence; $U_c(f)$ just has a maximum at the PW_A to PW_B crossover. This behaviour resembles rather the ion-doped HBCN1/6OO8 mixture, than the pure HBCN1.

Some further compounds, HBCN9 and HBCN10, though do not exhibit all the ‘banana-specific’ scenarios mentioned above, still possess the most unusual one: the PW_B up to very high f with $\frac{dU_c}{df} < 0$. HBCN9 has a speciality that the morphological sequence observed upon increasing the frequency is highly temperature dependent [40]. At the lower temperature part of the nematic phase, upon increasing f , in-plane longitudinal rolls (ILR) cross over to PW_B ; at higher temperatures, this sequence changes to conductive s-EC rolls—ILR— PW_B ; finally near T_{NI} , conductive s-EC rolls— PW_A — PW_B were observed. The ILR pattern found here is quite similar to the PW: it also involves alternating, in-plane director rotations; the periodicity is about the same ($\sim 2d$); however, its stripes are running parallel to \mathbf{n}_0 , in contrast to the perpendicular stripes of the PW. In HBCN10, PW_A is replaced by ILR in the whole nematic range (Figure 6). The complicated temperature—frequency scenarios of HBCN9 may be related to the fact that in this compound ϵ_a as well as σ_a depend on both the temperature and the frequency, involving sign inversion(s) too.

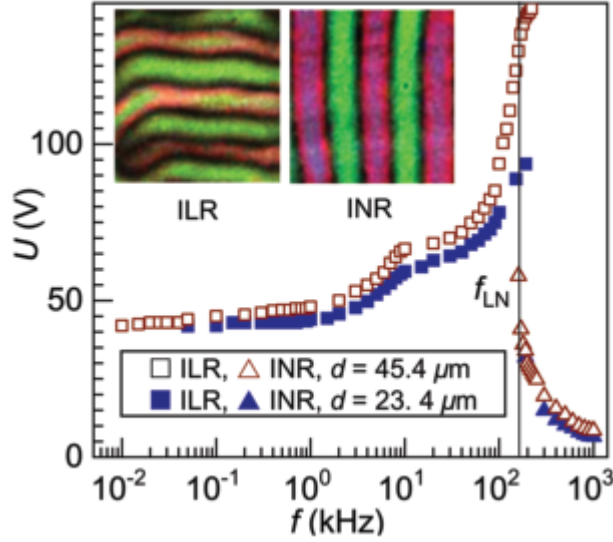


Figure 6. Frequency dependence of the optical threshold U_c at which the primary bifurcation into a patterned state is observed at $T^* = T/T_{NI} = 0.9623$ (the nematic-isotropic transition being at $T_{NI} = 401.5$ K) in samples of two different thicknesses. The crossover frequency f_{LN} separating the ILR and INR states is linear in T^* (between 0.95-0.99), represented, approximately, by $f_{LN} = 10728 T^* - 10134$.

Though, as we have seen above, ‘banana-specificity’ is not a unique property of a single specific compound, it is by far not general among BC nematics. For example, in the oxadiazole derivatives HBCN12-HBCN15 [42, 51, 52, 48] and in the bent-rod dimers DBCN3 [68, 69, 70, 71] and DBCN4 [72, 73], neither the two kinds of PWs, nor high f patterns with negative slope of $U_c(f)$ could be detected. Instead, the pattern morphologies observed resemble those found in calamitics. Patterns with their wave vector being perpendicular to (longitudinal rolls), parallel with (normal rolls, PWs) and enclosing an angle α (oblique rolls, $0^\circ < \alpha < 90^\circ$) with \mathbf{n}_0 were all observed. Remarkably, transitions between the various pattern types could be induced not only by the frequency, but also by voltage and temperature.

A speciality of the bent-rod dimers is that the combination of the calamitic and bent-core mesogenic parts generates in the compound such dielectric properties that are

not found in a BCN alone. Though typical BCNs have negative ε_a , DBCN3 belongs to the class (+, -), a combination which is quite rare even among calamitics, while DBCN4 exhibits a dielectric inversion, i.e., a transition from (-, +) class to the (+, +) class upon increasing the frequency. As a consequence, a planar DBCN3 sample requires a splay Freedericksz transition for ensuring proper conditions for the appearance of longitudinal ns-EC rolls [70]. In contrast, in homeotropic DBCN4 samples (above the dielectric inversion frequency) a bend Freedericksz transition results in a degenerate planar Freedericksz state, serving as a base for various secondary bifurcations (corresponding to normal rolls, defect mediated chevrons, broad domains, defect free chevrons and turbulence) observed at various f and U [72, 73]. Additionally, all the patterned states showed the travelling wave behaviour.

The compound HBCN12 needs a special attention, as it is one of the BC nematics that were claimed to exhibit a uniaxial N_u at higher, as well as a biaxial N_b nematic phase at lower temperatures [42]. At a fixed frequency of $f = 1$ kHz, in the N_u range, longitudinal rolls (originally misassigned as PW1) appear as the first instability, which changes to a PW pattern upon exceeding a second threshold voltage. This latter pattern prevails at decreasing the temperature even into the N_b phase, where longitudinal rolls are absent. The change in the direction of the wave vector of the primary instability was regarded as an indication of the N_u — N_b phase transition and was attributed to a change of the ratio of the elastic constants. While the latter claim may hold, even though the mechanism of how the elastic constants affect the wave vector is yet unexplored, the correlation between the changes of \mathbf{q} and a uniaxial—biaxial phase transition is questionable. As argued in Section 1, the existence of a thermotropic biaxial nematic phase has not yet been justified unambiguously; the observed apparent biaxiality in the N_b phase might have been mimicked by the uniaxial

nematic due to some changes in other conditions, like an anchoring transition or spatial dependence of the surface alignment [3]. While a purely temperature induced uniaxial-to-biaxial transition (at $U = 0$) is not probable in nematics, a similar transition could be induced in HBCN3 by a sufficiently large electric field [68, 69, 70, 71]. On the one hand, the field induced a metastable, biaxial basic state; on the other hand, the EC pattern emerging from this basic state had a 90 degree rotation of the wave vector compared to that in the uniaxial state (normal stripes instead of longitudinal ones). We note here that the dc field induced optically isotropic state reported for HBCN3 was also interpreted as a manifestation of field induced biaxiality [84].

Applying dc or low f ac voltages as excitation, may raise the question of polarity sensitivity of EC patterns. In the conductive regime of s-EC, the director modulation is independent of the polarity of the applied voltage, while in the dielectric s-EC regime as well as in the longitudinal ns-EC rolls, the director tilt flips to opposite direction upon a polarity reversal, which is hence equivalent to a half-wavelength shift of the pattern along the wave vector \mathbf{q} . Nevertheless, \mathbf{q} itself remains unaffected and, whether polarizing microscopy or a diffraction set-up is used for observation, at normal light incidence, optics does not discriminate between the upward or downward states of the director; thus the optical response of EC patterns should not be polarity sensitive.

A polarity sensitivity of \mathbf{q} might be generated using twisted cells, assuming that at onset, the pattern always appears close to one surface. Indeed, observations of a transient EC in a calamitic nematic indicated that the pattern develops close to the cathode rather than in the bulk; thus the wave vector is determined by the rubbing direction (\mathbf{n}_0) of the negative electrode of the twisted cell [85]. A similar polarity sensitivity of the wave vector of flexoelectric domains has also been reported in twisted cells of HBCN4 [35] and HBCN3 [32].

In light of the above considerations, it is quite surprising that in a planar sample of HBCN15 (where the rubbing directions are the same on both electrodes) a polarity dependent wave vector was observed at low f excitations (Figure 7). The two wave vectors, each corresponding to one of the two degenerate forms of oblique rolls, enclosed nearly an angle of 90° [52]. It is not yet understood, why and how one of the wave vectors of the oblique rolls is selected by the polarity, while in other BCNs and in calamitic materials the degenerate solutions are either superposed forming a grid pattern or exist side by side as a zigzag pattern.

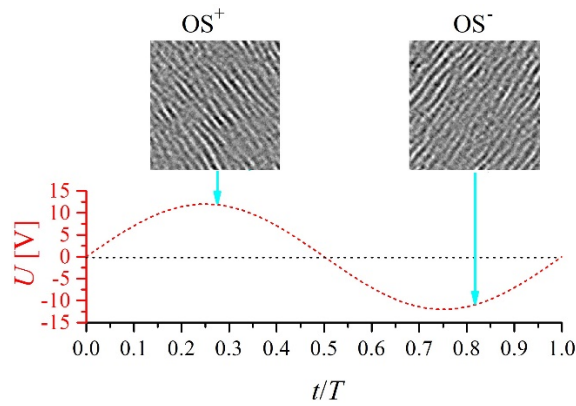


Figure 7. Snapshots of the oblique stripes in HBCN15 at their maximal contrast in the positive (OS^+) and in the negative (OS^-) half periods of the driving ac voltage of $f = 12\text{Hz}$, $U_0 = 8.3\text{ V}$. The vertical arrows indicate the time instant, when the snapshots with $70 \times 70\text{ }\mu\text{m}$ size were taken. The initial director \mathbf{n}_0 is horizontal, the crossed polarizers are at $\pm 45^\circ$. (After [52])

The EC scenarios described above represent extended patterns, capable to fill the whole overlapping electrode area. Under special (actually quite rare) circumstances only localized patterns extending to finite distances can be observed. Worms, i.e., patterns in regions narrow perpendicular to, but elongated along \mathbf{q} are the most common paradigm of such localized patterns. Worms were first observed in calamitic nematics

[86, 87], but may also exist in BCNs; they were actually observed in the higher temperature (regular) nematic phase of SBCN1, as exemplified in Figure 8. [55].

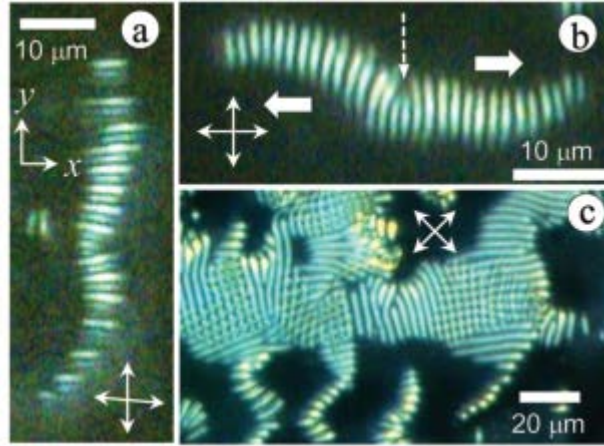


Figure 8. (a, b) Worms in SBCN1 appearing at the two substrates, at $U = 13$ V, $f = 45$ Hz, deep in the splay Freedericksz state; the wave vector of the worm is normal to the easy axis at the boundary where it forms. In (b), block arrows indicate the drift directions; dashed arrow points to the edge dislocation where new domains nucleate. (c) Extended state of worms at $U = 13$ V, $f = 40$ Hz. Double arrows indicate polarizers. (After [55])

3.2. Flexoelectric domains

Flexoelectricity plays a non-negligible role in electrically induced pattern formation of nematics. Flexoelectric torques can lead to spatially periodic, equilibrium director distortion of a nematic in the presence of an electric field. The result is a set of static, longitudinal parallel stripes, the flexoelectric domains (FDs), running along the initial, planar director alignment \mathbf{n}_0 . The pattern occurs as a consequence of the linear coupling between the electric field and the flexoelectric polarisation which yields a lower free energy in the deformed state compared to the undistorted one.

The first observations of FDs [88, 89, 90, 91] as well as a theoretical model [92] has been published in the 1970s in calamitic nematics. The model was based on the fact that splay and bend director distortions are associated with the flexoelectric polarization

described by two material parameters, the e_1 splay and the e_3 bend flexoelectric coefficients. This first, largely simplified model used DC driving, neglected the anisotropy of elasticity and the electrical conductivity. The director equations, originating from the torque balance could then be solved analytically in the linear regime of small distortions of the planar basic state. One obtained a threshold formula for the onset voltage of the FDs and for the critical wavenumber of the pattern [92].

The theory has later been extended to anisotropic elasticity [78], which resulted in a rigorous calculation of the existence region of FDs in terms of the relevant material parameters, namely the dielectric anisotropy ϵ_a , the elastic constants K_1 and K_2 , and the flexoelectric coefficients e_1 and e_3 . A further step was to extend the theory to AC driving, using numerical solution of the linear, torque balance equations. The analysis has been restricted to low frequencies, since in all experimental situations studied, FDs were replaced either by the equilibrium Fredericksz state or EC at higher frequency. A rigorous, nonlinear theory has also been developed [49], where the voltage dependence of the wave number q was calculated revealing an almost linear behaviour. The analytical calculation was confirmed by a numerical analysis of the full, nonlinear equations for the director field and the induced electric potential.

Experimental observation of FDs has been reported only for a limited number of rod-like nematics [93]. The reason is that the FD-forming mechanism requires a specific combination of the above mentioned material parameters, geometrical constraints and low conductivity (high purity), as well as low frequency driving.

Concerning bent-core materials, those of them, which exhibit nematic phase are expected to behave similarly to calamitics when subjected to electric field. Indeed, one frequently observes EC patterns, as discussed in the previous Section, as well as FDs. First observations of the latter in BCNs date back to early 2000s [36, 31].

The theoretical description of FDs worked out for calamitics do not need modification; the same model applies for FDs in BCNs. This is plausible, as far as the mesophase structure and behaviour are the same. A quantitative comparison of experimental results with the theory for BCN is, however, rare (or missing), since the measurements of the relevant material parameters are in most cases not available. Nevertheless, the study of FDs in BCNs reached a considerable interest due to the combination of the bent-core shape of the molecule with a transverse dipole moment component, which results in an ideal situation for a large flexoelectric response and thus enhances the formation of FD structures, even at higher electrical conductivity.

The magnitude of flexoelectric coefficients in BCNs is, however, a controversial issue. Due to their bent molecular structure, BCNs are anticipated to possess higher bend flexoelectric coefficient (e_3). Indeed, measuring the flexoelectric polarization directly by mechanical flexing of the bounding substrates, a giant e_3 , exceeding by about 1000 times the value in a common calamitic (5CB) was reported [14, 94]. This is, however, in a striking contrast with the results obtained by employing the classical, indirect measuring techniques [95], which yielded at most some mild enhancement of e_3 in BCNs or in mixtures of BCNs with calamitic nematics [96, 27, 97, 98, 99, 100, 101, 44, 102, 103]. Though BC nematics are achiral materials, their flexoelectric properties were often tested by adding a chiral dopant and measuring the flexoelectro-optic effect [104] in the resulting cholesteric phase. Measurements concluded in enhanced flexo-elastic ratios $e/K = (e_1 - e_3)/(K_1 + K_2)$ in the conventional nematic phase of soft-core BCNs [105, 106, 107, 108, 109, 110, 111, 112, 113]; the increase of e/K is even larger in the N_{TB} phase [114] reaching a factor of 40 in SBCN1 [115], which is still much lower than the giant value mentioned above.

The reason for this discrepancy lies in the nanostructure of BCNs. While e_3 might have a theoretical upper limit (much less than the giant e_3) in a homogeneous nematic medium [116, 117, 118], BCNs with a cybotactic nematic phase cannot be regarded homogeneous in this respect. Besides the dipolar and quadrupolar molecular contributions to flexoelectricity, in these BCNs, reorientation of the cybotactic polar smectic clusters provides another, much larger contribution to e_3 , resulting in the giant value [98, 94]. The cluster reorientation can be activated by the flow induced by mechanical flexing of the substrates, as well as by exceeding a high, critical electric field, realised during demonstration of the converse flexoelectric effect [119]. Whenever the electric field does not exceed this critical value (as is assumed for the classical, indirect flexoelectric measurements in cell with non-flexible substrates), only the molecular contributions can be detected without the contribution of the clusters, thus explaining e_3 values in similar order as that of calamitic nematics. This applies also for the flexoelectric coefficients determined from the characteristics of FDs [120, 27], indicating that during the formation of FDs the cluster contributions to flexoelectricity do not play a role.

There is a further problem though with the identification of the patterns, as a clear distinction between EC and FDs is not straightforward. A rough approach is to look just at the mutual direction of the wave vector \mathbf{q} and the initial director \mathbf{n}_0 , searching for parallel stripes (Figure 9). This usually works in calamitics, because longitudinal EC rolls (a kind of nonstandard EC) mostly do not occur at low frequencies, where FDs are observed, thus a direct transition from FDs to longitudinal ns-EC rolls is rare. In contrary, in BCNs, due to the higher bend flexoelectricity, FDs occur in a broader parameter range and, at the same time, longitudinal ns-EC rolls are more frequent, creating an opportunity for an overlap or a direct transition between the

two, like in HBCN1 [120, 27] or HBCN12 [42, 43, 44]. Consequently, for a clear identification of FDs one needs to study the nonlinear behaviour, by measuring the wavenumber as a function of the applied voltage. Experimental observation of possible FDs in BCN has first been mentioned for HBCN5 [36] and HBCN2 [31], though without an attempt to rigorously identifying the structure.

Later this has been done for a few cases: HBCN8 [38], HBCN4 [33], HBCN13 [46, 50] and HBCN3 [32]; namely, the voltage dependence of the wave number, as a characteristic feature of FDs was detected and a linear increase was found similarly to the calamitics (see Figure 9(a)-(c) and Figure 10).

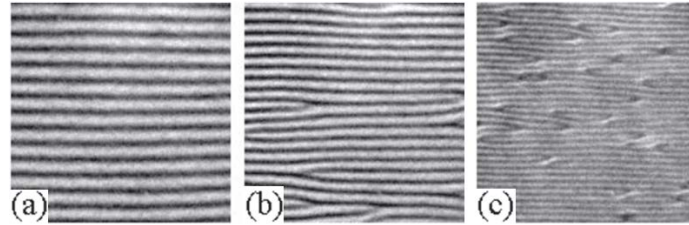


Figure 9. Snapshots of dc voltage excited flexoelectric domains in HBCN13 (a) near the threshold ($U = 23$ V), (b) at $U = 28$ V, (c) much above threshold ($U = 45$ V). The initial director \mathbf{n}_0 is horizontal. (After [48])

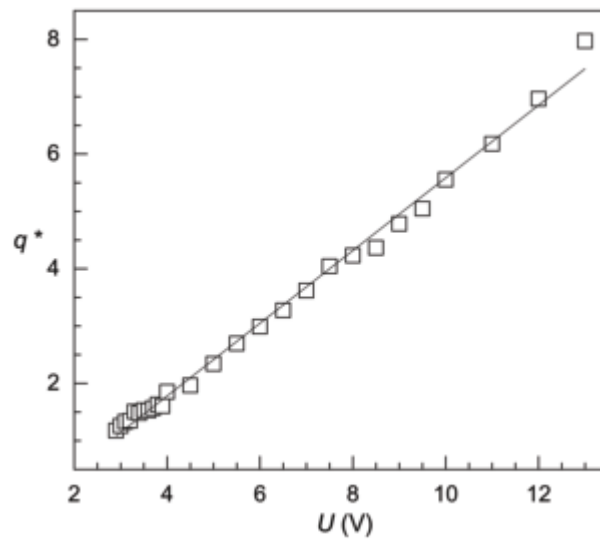


Figure 10. Voltage dependence of the dimensionless wavenumber $q^* = q d/\pi$ of FDs in HBCN4. (After [33])

More detailed experimental studies in planar cells of HBCN13 have been reported in [45, 47, 48, 50].

A crossover from FDs to EC was found and characterised at very low (below 1 Hz) frequencies, where both patterns exhibit flashing character due to the fact that the director relaxation time is shorter, than the period of the driving voltage. Frequency and voltage dependence of the pattern morphologies as well as their dynamics within a single period were also studied [45]. From the intensity and phase of the diffracted laser beam, it was concluded that the structure is very similar to that of calamitic nematics and is not sensitive to changes in the material parameters. Diffraction measurements revealed another specific feature of FDs, namely that the polarisation direction of the first order diffracted light is perpendicular to that of the incident laser beam. This is the consequence of the 3D deformation of the director, involving a periodic modulation of both the tilt angle and the azimuthal angle of the director [45].

A further insight into the 3D structure and dynamics of FDs was gained by studying HBCN4 in twisted cells. Experiments were done in initially 90°-twisted planar configuration excited by a low frequency, square wave electric field. The flexoelectric modulation appeared close to the cathode at each polarity reversal and, at low voltage amplitudes, decayed completely as the field became steady. Correspondingly, at successive polarity changes, the FD stripe direction switched between the alignment directions at the two substrates. For large voltages, the stripes formed nearly along the alignment direction at the cathode and gradually reoriented toward the midplane director. These observations were generally attributed to inhomogeneous and time-dependent field conditions that occur after each polarity reversal [35, 55].

3.3. Periodic patterns as gratings for optical devices

Experimental as well as theoretical studies of periodic patterns have been motivated by multiple aims. One principal task is the understanding of the mechanism of the pattern formation, which still has remained a great challenge for many bent-core substances. Another task is the proper description of pattern characteristics (morphologies, threshold voltages, etc.) that we mainly focussed in the above sections. A third motivation could be the application of the phenomena in optical devices, which is made possible by the fact that periodic patterns (whether EC or FDs) correspond to an optical grating (typically a phase grating). In such applications, besides calamitics also BCNs or mixtures of BCNs with calamitics can have grate potential.

Using EC, with a proper combination of the amplitude and frequency of the applied ac voltage, the direction of the wave vector and to some extent also its magnitude can be adjusted. It has been shown that by adding SBCN1 to the ionic-salt-doped, commercial nematic mixture MLC 2081, the range in which the wave number can be tuned by the frequency of the applied voltage could be substantially extended, both towards lower and higher q values [121]. This improvement has been attributed to the change of the elastic moduli (especially to the reduction of K_3) occurring as a consequence of doping with the soft-core BCN.

In case of FDs, though the direction of the wave vector is fixed by the surface orientation, its magnitude may be tuned linearly with the applied dc voltage. Tunable optical gratings based on FDs have been created from HBCN13 [45, 47] and it was shown that they are potential alternatives of current methods for laser scanning or beam steering applications, especially, where the small size, the simplicity and low cost of the tunable optical grating device is important. Compared to current solutions like piezoelectric scanning mirrors or acousto-optic modulators, an FD-based device is

simpler, it has no moving mechanical parts, the operating voltage is low, with convenient linear characteristics. It was shown, that the wave number (the periodicity for the grating) is linearly adjustable in a wide range of a dc voltage. The wave number adjustment occurs via defect generation and annihilation, where the switching time is larger for lower wave number initial states [47, 48].

A novel type of BCN molecules, HBCN16 [53], containing a photosensitive moiety opened a way towards light tunable optical gratings based on FDs. The grating characteristics can be controlled by combining the effects of the pattern driving electric field and light illumination. The combination of the electric and optical fields opens new dimensions for the applications. The number of control parameters is higher: apart from the amplitude and frequency of the electric field, one is able to vary the wavelength and the intensity of the light as well as the duration of the illumination. The light tunability is ascribed to the photoisomerization effect of the azo moiety in the BCN molecule. The *trans*-to-*cis* isomerisation induced by a UV (365 nm) irradiation, as well as the *cis*-to-*trans* back-relaxation forced by blue (457 nm) light illumination changes the ratio of trans and cis isomers yielding a shift of the phase transition temperatures (the nematic range) and altering the dc threshold voltage and the critical wave number of FDs in HBCN16. Based on this principle, a prototype of a controllable optical grating was assembled capable to be operated either as a light controlled shutter switching light beams on/off or be used for beam steering via changing the wave number and thus the diffraction angle of FDs. Due to the easy, instant and remote operation by light, this device allows a contactless tunability, providing great advantage over the traditional, mechanically or electrically controlled photonic gratings [53].

Another way to create complex patterns for photonic devices is using photoalignment instead of the conventional rubbed polyimide technique. An example of

producing patterns by combining EC in HBCN13 and photopatterning has recently been reported [122].

4. Defects

Defects in an ordered medium are generally an outcome of local symmetry breaking. For example, line defects or *disclinations* that appear in the Schlieren texture of degenerate planar nematic layers involve breaking of continuous rotational symmetry. Equilibrium director fields around such disclinations are derived, in one elastic constant (K) approximation, by minimizing the volume integral of elastic energy density $F = \frac{1}{2}K(\nabla\mathbf{n})^2$, which requires $\nabla^2\beta = 0$, β being the azimuth of the director \mathbf{n} [Figure 11(a)] at polar angle α ; this, in turn, implies $\beta = s\alpha + c$, c being a constant and $s = \pm 1/2, \pm 1, \pm 3/2, \dots$ the strength or topological charge of the defect representing the angle through which \mathbf{n} rotates in going around the defect line; half-numbered defects ($s = \pm 1/2, \pm 3/2, \dots$) are a consequence of the equivalence $\mathbf{n} \equiv -\mathbf{n}$. Interestingly, unlike in rod-like nematics, in HBCNs and SBCNs, a direct optical visualization of defect geometries is possible, as demonstrated in Figure 11(b). This feature is analysed in [123] as due to quasiperiodic microscale surface modifications brought about by nanometric clusters intrinsic to bent core systems. Apart from disclinations of the *wedge* type that run parallel to the rotation vector as in Figure 11, it is possible to have *twist* lines lying orthogonal to the rotation vector. Twist loops carry no topological charge.

Defects in the form of *edge dislocations* arise in periodic structures, such as arrays of convection rolls or flexoelectric domains, electrically generated in nematics. They break the discrete translational symmetry. We may associate a topological charge Q with such a dislocation, defined by

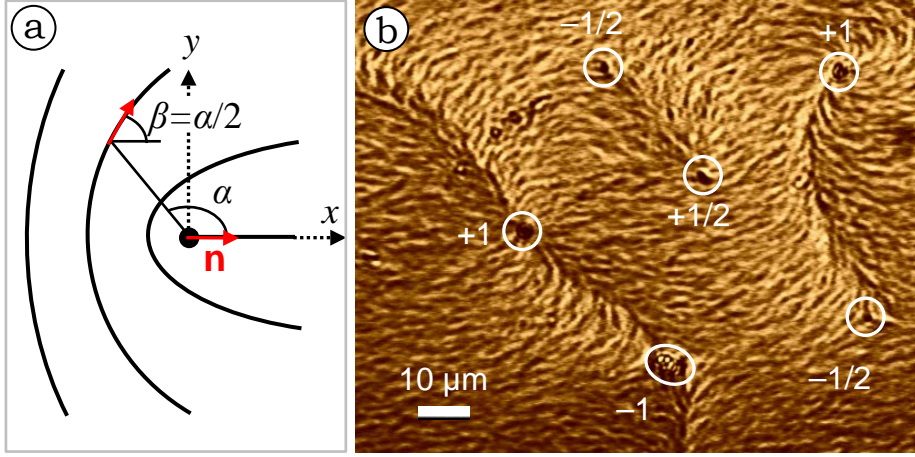


Figure 11. (a) Schematic of \mathbf{n} -field around a $1/2$ -strength disclination along z in a degenerate planar nematic with $\mathbf{n} = (\cos \alpha, \sin \alpha, 0)$. (b) Configurations of the inplane director normal \mathbf{n}_\perp around various disclinations located at the encircled nodes in nematic SBCN1 at 1°C above the N - N_{TB} transition temperature, as seen by an optical microscope. (After [123]).

$$Q = \frac{1}{2\pi} \oint \mathbf{q} \cdot d\mathbf{s} = \pm 1, \quad (1)$$

where \mathbf{q} is the wave vector given by the gradient of the phase variable. The sign of the dislocation may be chosen as positive when, in circumnavigating the defect in an anticlockwise manner, one ends up with an added pair of rolls [39].

Point singularities, also referred to as hedgehogs, are unique to bulk nematic samples [124]. For example, in a large nematic drop of radius $R > K/W$, with homeotropic surface anchoring of strength W , the director distribution is radial everywhere outside a point singularity of charge $+1$ residing at the centre. This point defect can open out into its topologically equivalent $+1/2$ disclination loop. The antidefect of a radial hedgehog is a hyperbolic hedgehog of charge -1 that is equivalent to a $-1/2$ loop. These point defects and their association into dipoles are of particular relevance to nematic colloids [125, 126].

Analogous to Neel walls and Bloch walls of magnetic systems, we have dielectrically or diamagnetically created Brochard-Leger walls [127] in nematics. In particular, during an electric Freedericksz transition, since the dielectric torque is quadratic in field \mathbf{E} , the director tilt can be positive or negative with equal probability. Regions of opposite tilt are bridged by walls within which the tilt changes smoothly. The distortion in the walls, depending on the geometry, may be predominantly of the splay, bend or twist type.

4.1. Defects in patterned electroconvective states of BCNs

As noted in Sec. 3.1 (Figure 4), the defining electroconvective states of HBCN compounds manifest optically as prewavy patterns PW_A and PW_B that appear, at threshold, as translationally invariant array of stripes, with a periodicity λ_p equal to the separation of alternate stripes ($\sim 3d$). This period begins to decrease linearly as the applied voltage U is gradually increased above U_c . A rapid increment in U often leads to nucleation of edge dislocations, thereby rendering λ_p to be lower than its equilibrium value. Wiant et al. [25], who were the first to notice these features in the prewavy patterns of HBCN1, identify two main types of dislocation of which one involves bifurcation of a single stripe and the other, crossover of two stripes. By an abrupt large jump in U , a multiple defect state, termed the knitting instability, is obtained; see Figure 12.

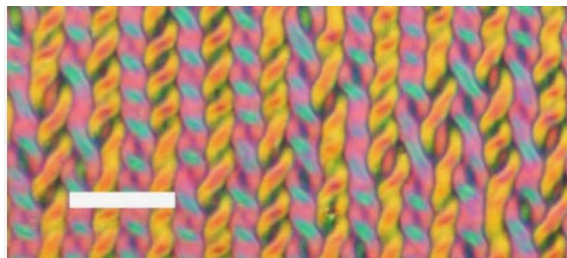


Figure 12. The “knitting” instability at 40 kHz and 35 V. It is produced by abruptly raising the voltage in one of the prewavy states. Image taken with a 10 μm sample of HBCN1 at 70 $^{\circ}\text{C}$ between crossed polarizers that were rotated 15 $^{\circ}$ with respect to the

vertical direction in the picture. The rubbing direction of the cell plates is in the horizontal direction in the picture; scale bar: 100 μm . (After [25])

A later study [39] on HBCN9 analyses the formation, dynamics, and annihilation of edge dislocations of opposite topological charge ± 1 in the prewavy state, alternatively described by therein as the inplane normal roll (INR) state. To locate the defect position accurately, the INR pattern is represented by $\psi(x, y) = A(x, y) \exp(iqx) + \text{c.c.}$, where $A(x, y)$ signifies the complex amplitude field. A complex demodulation method [128, 129] is used to extract $A(x, y)$ from the roll pattern; after removal of the underlying periodicity, the defects are located at the intersection of real and imaginary parts of $A(x, y)$, where the absolute value of $A(x, y)$ is zero and the phase is undefined. Figure 13(a) exemplifies the result of this procedure. The approach of paired (i.e., having a roll in common), oppositely charged defects toward each other is found to be a two-step process marked by near constant velocity at large separation and accelerated motion close to annihilation, as in the case of nematic rolls belonging to standard EC; see Figure 13(b) and 13(c). Upon a sudden, strong elevation of the control parameter $\varepsilon = (U^2 - U_c^2)/U_c^2$, periodic arrays of dislocations of alternating polarity form. The chevron structure that appears between undulatory defect chains as in Figure 14(b) may be identified as the knitting instability shown in Figure 12.

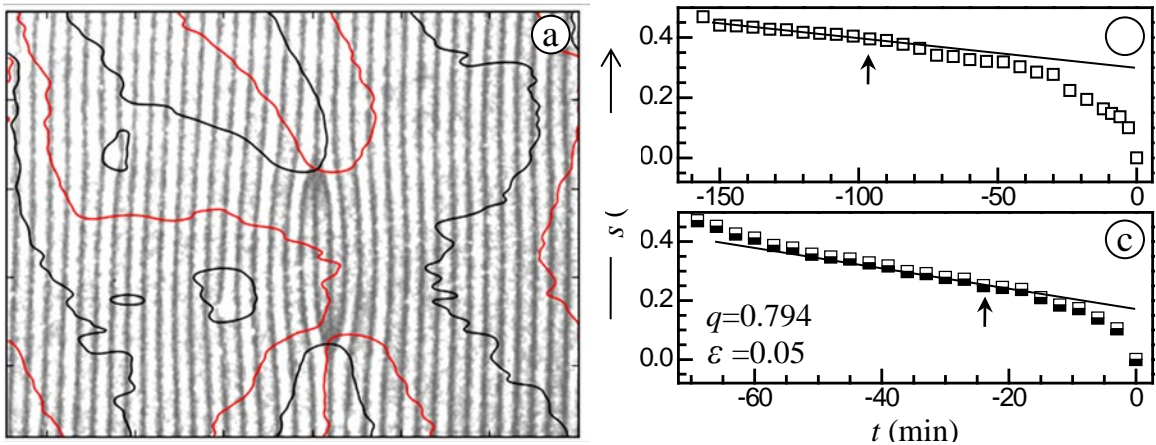


Figure 13. (a) Plot of $\text{Im}A = 0$ (black lines) and $\text{Re}A = 0$ (red lines) superimposed on the INR pattern in grey scale; the black and red lines intersect at the paired dislocations. (b, c). Time variation of the separation between paired defects approaching each other toward annihilation at $t = 0$. Arrows indicate the distance below which the motion is accelerated. Lines through the points just outside the range of acceleration are of slope increasing with q . The range of acceleration decreases with increasing q . It is q rather than ε that is the key parameter determining the dynamics. (After [39]).

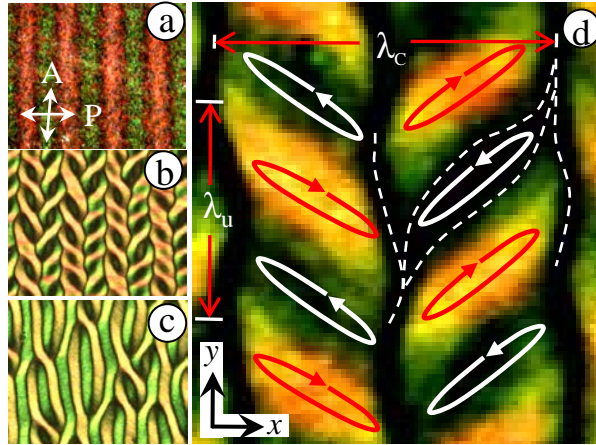


Figure 14. Formation and relaxation of metastable chevrons in supercooled nematic HBCN9. (a) Inplane normal roll state near the threshold; control parameter $\varepsilon = 0.14$. (b) Chevrons formed a few seconds after suddenly increasing ε to ~ 28 . (c) The usual edge dislocation state to which the chevron state in panel (b) has relaxed after 200 s. $d = 15.5 \mu\text{m}$, $f = 50 \text{ kHz}$, $T = 80^\circ\text{C}$; Analyzer A at 85° relative to polarizer P. (d) Schematic representation of the vortex lattice corresponding to the chevron texture; dotted lines outline a pair of oppositely charged dislocations. λ_c is the period of the chevron superstructure along x and λ_u is the period of the undulatory line between adjacent chevron bands. (After [39]).

The flow field associated with chevrons is mainly *inplane* as indicated by the vortical trajectories of foreign particles suspended in the fluid. The overall flow pattern constitutes a vortex lattice as schematically presented in Figure 14(d). The chevron structure is metastable and decays with time. The relaxation of chevrons, which may be

considered equivalently as a gradual ‘melting’ of the vortex lattice, is accompanied by an exponential reduction in the dislocation density; see Figure 15. The initial periodicity of defect chains also drops exponentially with increasing field.

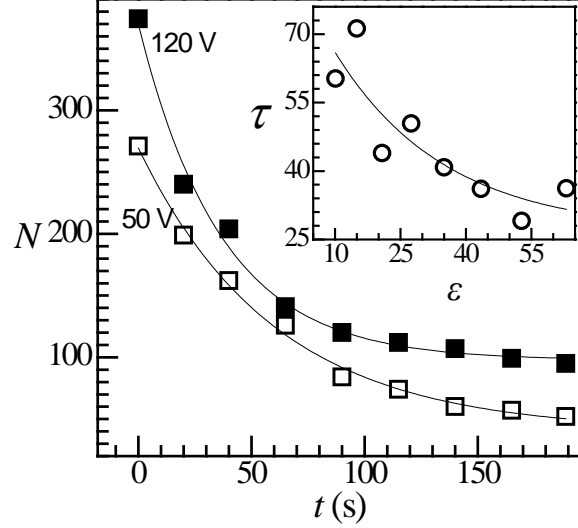


Figure 15. The number of edge dislocations N in a $320 \times 210 \mu\text{m}^2$ area of the sample as a function of time. The data are from the images of relaxing chevrons captured over 200 s, with an interval of 1 s between successive images. The time $t = 0$ corresponds to that of fully developed chevron state or maximum dislocation density obtained after a few seconds of switching V from 16 V to the voltage indicated. Inset: Relaxation time τ as a function of control parameter ε ; the continuous line indicates $\tau(\varepsilon)$ to be broadly an exponentially decreasing function. (After [39]).

Under increasing constraint, the formation of metastable edge dislocations in the prewavy structure is followed by nucleation of loop disclinations that mediate in the development of the final turbulent state [40, 13], as in the dynamic scattering mode of standard EC [130]. However, unlike in the latter case, the loops here are highly ordered with regard to their spatiotemporal behaviour. In all the three inplane roll states (ILR, INR2 and INR1), when the amplitude of azimuthal modulation becomes very large, the unperturbed regions, seem to acquire a π -twist across the sample thickness to reduce energy. This would lead to the formation of half-strength twist disclination loops

separating the twisted and untwisted zones. With increasing constraint, the loops collapse laterally, along the wave vector, into line defects with the end regions remaining semicircular. They are spatially well coordinated with the gradient in azimuthal deviation, i.e., $d\phi/dy$ for the ILR and $d\phi/dx$ for the INR; they form along alternate lines of zero gradient, where the curvature, $d^2\phi/dy^2$ for the ILR and $d^2\phi/dx^2$ for the INR, has the same sign, thus breaking the sinusoidal symmetry of the azimuthal field. Disclinations corresponding to opposite curvatures occur in separate zones and those in a given zone drift continually along a common direction. For example, in the case of the INR, they drift along y or $-y$ depending on the sign of $\phi(x)$ -curvature at their location. Figure 16 provides examples of disclinations formed in the ILR and INR states. Figure 17 pertaining to the INR2 state in HBCN9 depicts the voltage variation of average defect speed v_d determined from time series recordings for various constraints at a fixed frequency. Interestingly, v_d , which tends to saturate till about $1.5 U_{cd}$ ($U_{cd} \approx 55$ V denoting the defect threshold), exhibits an ever-increasing trend in the high voltage region. This is possibly related to the process of collapse of the loop defects into narrow disclinations occurring over an extended voltage region. The inset in Figure 17 depicts the exponential growth of mean area density of the defects ρ_d (determined using time images of size $510 \times 520 \mu\text{m}^2$) as a function of U . At very high voltages, the loops become numerous and their motion increasingly random leading to the chaotic state.

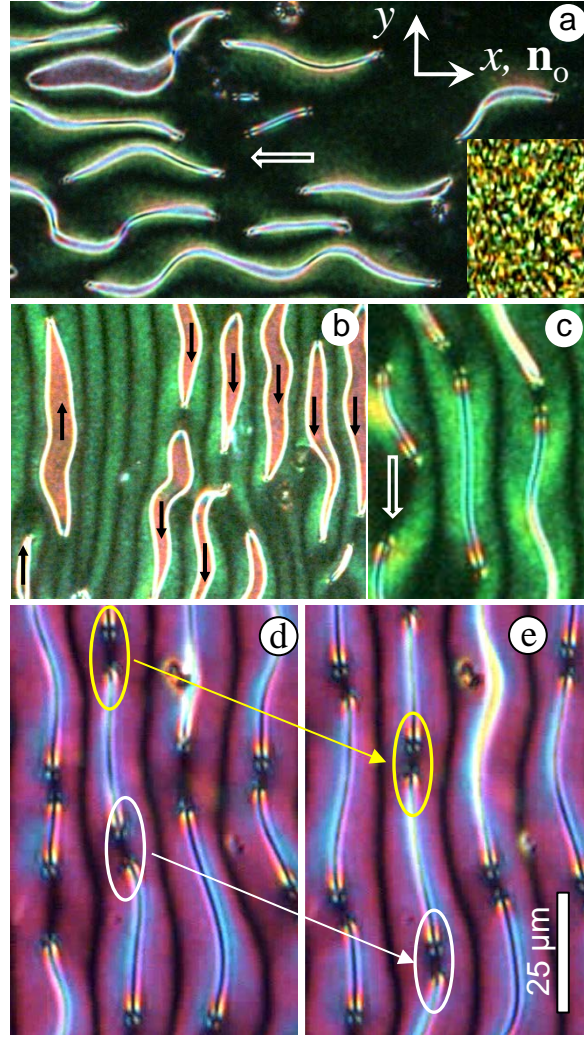


Figure 16. Drifting disclinations. (a-c) A planar 12.7 μm -thick-layer of HBCN10 at $T = 0.9527 T_{\text{NI}}$; (a) leftward moving disclinations in the ILR state; 1 kHz, $1.15 U_c$; inset: dynamic scattering state, $4.63 U_c$; (b) upward and downward moving loops in the INR state; 0.5 MHz, $3.36 U_c$; (c) as (b), laterally collapsed loops, $3.4 U_c$. (d, e) INR2 state in a planar 16 μm -thick-layer of HBCN9; frames captured 6 s apart, showing the downward drift of disclinations; sloping arrows are drawn between corresponding regions; $T = 0.9608 T_{\text{NI}}$; 5 kHz, $1.3 U_c$. Crossed polarizers along (x, y) . (After [40, 13])

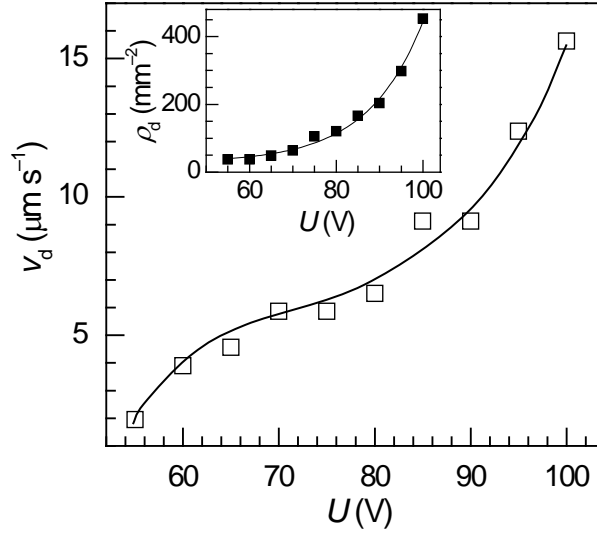


Figure 17. Average drift speed v_d of disclinations formed in the INR2 state, along the y direction. Inset: area density ρ_d of loop disclinations as a function of voltage; $T=0.9608 T_{\text{NI}}$, $f=5$ kHz, and $d=16.2$ μm . (After [13])

4.2. Defects in the patterned flexoelectric state of BCNs

In [36, 38], an unusual smectic-fan-like texture is reported for the planar nematics HBCN5 and HBCN8 in high static electric fields. The course of structural changes that leads to this morphology is analysed in detail in HBCN4 [33]. It is related to dislocations or, equivalently, disclination pairs developing under increasing electrical stress in the Bobylev–Pikin flexoelectric domain pattern. Half-strength disclinations of opposite topological charge evolve within the flexo-structure rendering the wavevector orientation degenerate in the layer plane. Dipolar and quadrupolar topological defect patterns, akin to the singularities in cholesteric fingerprint texture, lead finally to fan like objects; see Figure 18(a)-(e). The morphological equivalence between the periodic flexoelectric state and a layered lattice thus realized is attributed to a much lower energy of bend type distortion compared to splay, unlike in a calamitic. In a related study on HBCN3, Elamain et al. [32] find the electrooptic characteristics of polymer-stabilized flexo-domain pattern

to be quite similar to that of short pitch cholesteric (in the uniform lying helix state) and ferroelectric liquid crystals. They interpret this result as indicative of a heliconical-like molecular order present in the flexoelectric patterned state.

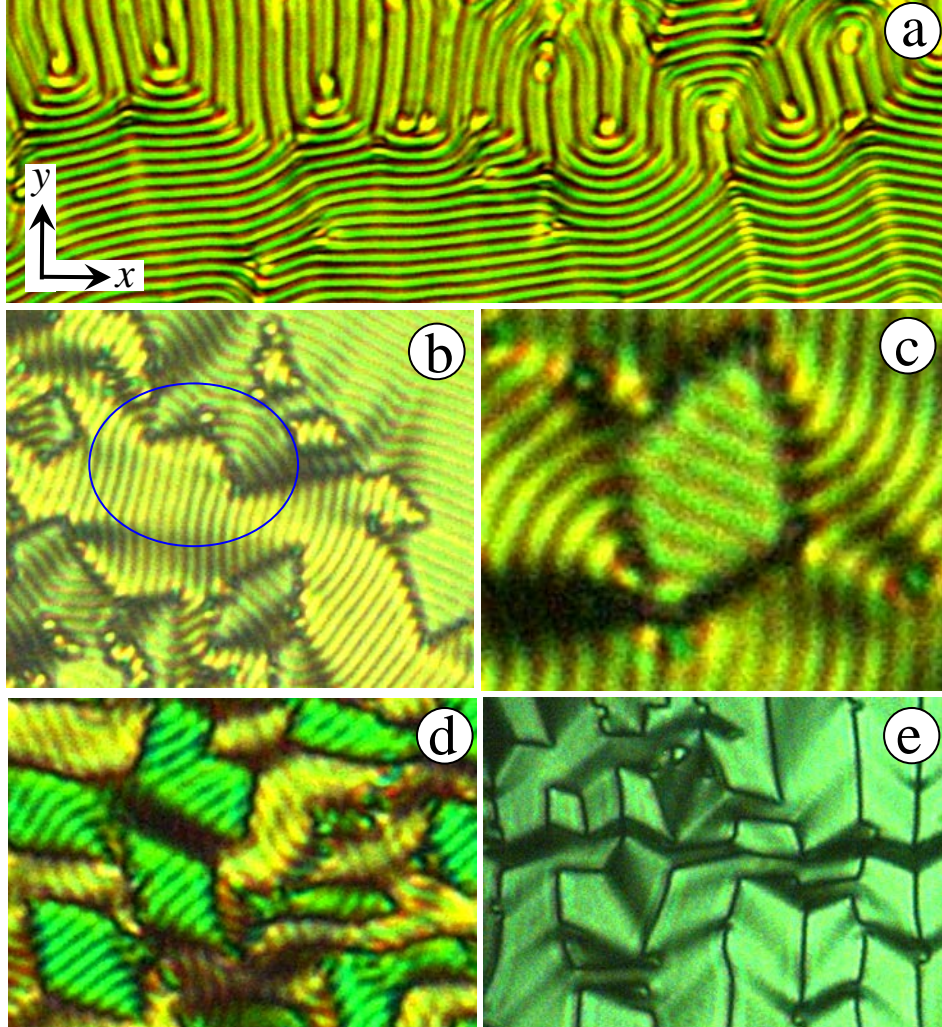


Figure 18. Various disclination geometries of the flexodomain pattern excited by high static fields. (a) An array of alternately positive and negative π -disclinations as seen with a single polarizer along y . (b) Zig-zag extinction lines seen under crossed polarizers; they join positive and negative defects occurring alternately at the turning points. (c) Angular quadrupole due to two positive and two negative π -disclinations at the corners of a quadrilateral. (d) A network of quadrupoles as seen using crossed polarizers with a full-wave plate. (e) A region mostly filled with angular quadrupoles (fans) at twice the threshold voltage. (After [33])

4.3. Field-induced point-, line- and wall-defects in BCNs

In [37], Krishnamurthy et al. examine the stability of electrically generated half-strength twist disclination loops separating planar and π -twisted regions in planarly anchored nematic HBCN7. Loops L(P) and L(T) enclosing planar and π -twisted domains, respectively, are both generated during relaxation from the quasi-homeotropic splay-Freedericksz state. It is demonstrated that the metastable twisted state occurs as a rule in the region of lateral separation of singular loops that form via pincement of Brochard-Leger walls [127] and collapse at different rates; see Figure 19(a) and 19(b). These loops are readily distinguished from electroconvection roll patterns, as in Figure 19(c) and 19(d). The results provide the first experimental confirmation of the early theoretical prediction by Friedel and de Gennes [131] that, for circular loops L(P), there exists a critical radius R_c separating regimes of growth and decay. In Figure 19(e)-(h) showing loops L(P), loop 2 corresponding to R_c is in unstable equilibrium; loop 1 with $R < R_c$ decays in time, while loop 3 with $R > R_c$ enlarges. The Sonnet-Virga model for the dynamics of L(T) [132] is extended in [37] for the case of L(P); the resulting Eq. (1)

$$\frac{t_r - t}{\tau} = a_2(r_r - r) + (a_1 a_2 - a_3) \ln \frac{r_r - a_1}{r - a_1} \quad (1)$$

is found to agree well with the experimental data on the time variation of R . Here the coefficients a_i are determined by, apart from different numerical constants, a common geometrical parameter involving the defect core radius and sample thickness d , τ is the relaxation time dependent on the rotational viscosity γ_1 and effective elastic constant k , t_r is the reference time at which the scaled radius is $r_r = 2R/d$.

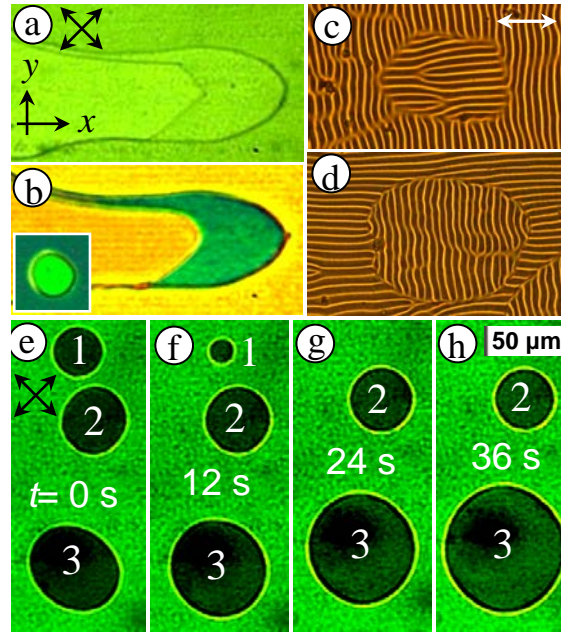


Figure 19. Formation and dynamics of twist loops in initially planar nematic HBCN6. (a) A pair of disclination loops (partly shown) formed from wall-pincement; 15 V, 10 kHz, 120 °C; (b) Same region soon after switching the field off; the green region is developing a π -twist; the inset, recorded a few seconds later shows the twisted circular domain (bright green) as it collapses. (c) s-EC rolls in π -twisted inner and untwisted outer regions separated by a *normal* twist loop, and (d) s-EC rolls for the case of inner planar and outer twisted regions separated by an *inverse* twist loop; 20 kHz, 9.5 V, 115 °C. (e-h) Inverse twist loops in different dynamical states at times t after removal of the field. Of the three loops, 1 is collapsing, 2 is critically stable and 3 is enlarging; 130 °C. Polarizers are indicated by double arrows. (After [37])

In their electro-optical study, Krishnamurthy et al [56] have examined the stability of the homeotropic state of the N_{TB} phase of SBCN1. By subjecting an initially planar (untwisted or 90°-twisted) nematic layer to an electric potential well above the Freedericksz threshold U_F and then cooling it, they derive the homeotropically aligned N_{TB} phase. This N_{TB} state, however, is metastable (except at very high voltages), lasting for a time governed by the applied voltage and temperature. Two different structural modifications are identified by which the homeotropic state of N_{TB} is destabilized. First of these manifests as a pattern of parallel stripes without any periodicity and forming

near the two substrates, extending along the normal to the rubbing direction at the substrate, where they form as in Figure 20(a); they involve splay deformations of the twist director and are polarity sensitive by virtue of the flexo-polarization associated with their structure; these features reveal the stripes as oily streaks of the type known in layered (smectic A) and quasilayered (cholesteric) systems; see inset in Figure 20(a). In dc fields, the stripes exhibit flexoelectrooptic-like effect, showing a slight deviation from being orthogonal to the rubbing axis R , with the sense of deviation dependent on polarity. The second mode of destabilization of the homeotropic N_{TB} alignment is through evolution of torical focal conic domains, TFCDs, which again are unstable; they transform into parabolic focal conic domains, PFCDs, with the parabolae in the vertical planes; this transformation can occur either through a process of continued dissociation of TFCDs, as in Figure 9(b)-(e), or upon the growing TFCDs coming into contact. The paper [56] outlines the application of extended Volterra process for an understanding of the formation and relative stability of defect structures in the N_{TB} phase. In a continuing study [57], an explanation is provided for the instability of TFCDs and the stability of PFCDs in the N_{TB} phase, as arising by reason of the presence (the first case) or absence (the second case) of defect densities attached to the conics, which are disclinations.

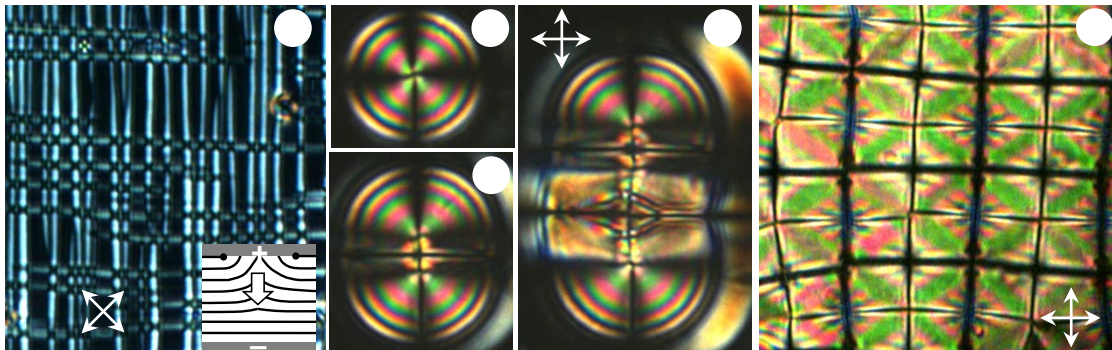


Figure 20. (a) Cross-hatched pattern of focal lines developed in a uniformly homeotropic 20 μm thick layer of SBCN1 held in a 90°-twist cell and rapidly cooled

through 0.5 °C below the N_{TB} setting point, under a $1 \text{ V } \mu\text{m}^{-1}$ sine wave field of frequency 1 kHz. Inset: Classic structure of oily streaks (of net zero Burgers vector) as paired $+1/2$ wedge disclinations attached to the top substrate. Block arrow gives the direction of net flexoelectric polarization when the field is downward. (b-d) Continued dissociation of a toric domain leading to the formation of a series of PFCDs; these frames are from a time series covering 150 s and recorded after reducing the voltage from 10 V to 1 V at 1 kHz; (e) A network of PFCDs formed eventually under an electric field; 8 V, 1 kHz; 20 μm thick planar layer. Double arrows show the axes of polarizers. (After [56]).

In the context of defect mediated dielectric reorientation in the N_{TB} phase, we may note that a dielectrically negative N_{TB} mixture, in the initial homeotropic configuration, has been found to undergo a heterogeneous bend-Freedericksz transition that is marked by the nucleation at isolated sites of axially symmetric or toric focal conic domains; above the threshold voltage, these domains begin to grow sinuously through splay and saddle-splay deformations of the optical axis [23].

In their splay Freedericksz experiments with a bent-rod type nematogen DBCN3, Stannarius et al. have observed [69, 68] a field-induced metastable nematic state that, after the field is switched off, coexists with the original uniaxial nematic state N_u for about an hour. The authors interpret the new state, preliminarily, as the biaxial nematic state N_b , particularly since it is also found in homeotropic cells. Characteristic inversion walls, exemplified in Figure 21, are observed to form in the relaxing N_b regions after removal of the field. The Brochard-Leger walls [127] are further seen to reflect unusually large shape anisotropy as compared to similar walls in calamitic nematics. The wall shapes are explained by assuming that the bend elastic constant K_3 is an order of magnitude larger than the twist constant K_2 , and that the flexoelectric contribution to the deformations is negligible.

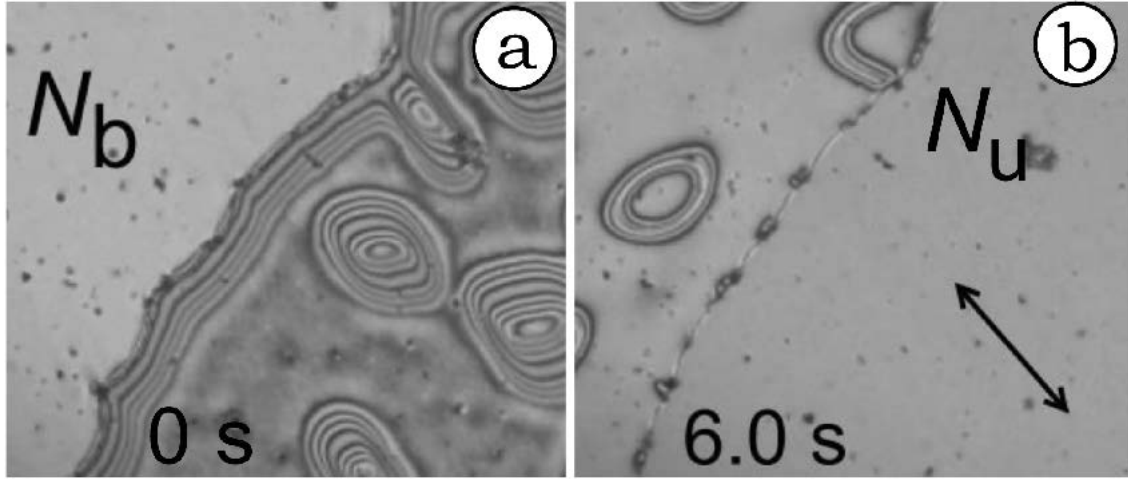


Figure 21. Walls in coexisting uniaxial nematic N_u and metastable biaxial nematic N_b domains in a 25 μm thick planar cell (with rubbing direction along the double arrow); time images with an interval of 6 s, captured after switching the field off from the splay Freedericksz state at 7.35 V, 1 kHz. The Brochard-Leger walls seen in the N_u region of (a) have disappeared in (b) and the sample has returned to the planar base state; in the N_b region in (b), walls of a new type, not present in (a), have formed. Reprinted figures with permission from [Stannarius R, Eremin A, Tamba M-G, Pelzl G, and Weissflog W. Phys. Rev. E 76, 061704, 2007] Copyright 2007 by the American Physical Society.

A recent study by KSK et al. [60] dwells on two electrokinetic phenomena associated with topological dipoles. The dipoles comprise N_{TB} drops acting as radial hedgehogs of charge +1 and their companion hyperbolic -1 defects; they form in the N - N_{TB} biphasic region of some binary mixtures of SBCN1 with a small quantity of a surfactant [i.e., 1-tetradecanoic acid (TA), 2-octadecoxypynol (OP) or 2-hexadecoxybutanol (HB)]. It is found that (i) the hyperbolic hedgehogs of elastic dipoles shift toward the negative electrode in static fields and perform oscillatory motion in AC fields, indicating the presence of nonvanishing flexoelectric polarization in the field-free state [Figure 22(a)-(c)]; (ii) the elastic dipoles, propelled by forces of backflow due to coupled flexoelectric and dielectric distortions, drift uniformly along their axes with the N_{TB} drops in lead [Figure 22(d)-(f)]; (iii) the translational velocity v_d

increases linearly with both f and the diameter of N_{TB} drops; and (iv) with increasing applied voltage U , $v_d(U)$ exhibits a monotonic, slightly nonlinear variation at $f = 200$ mHz, tending toward linearity at higher frequencies; see Figure 23.

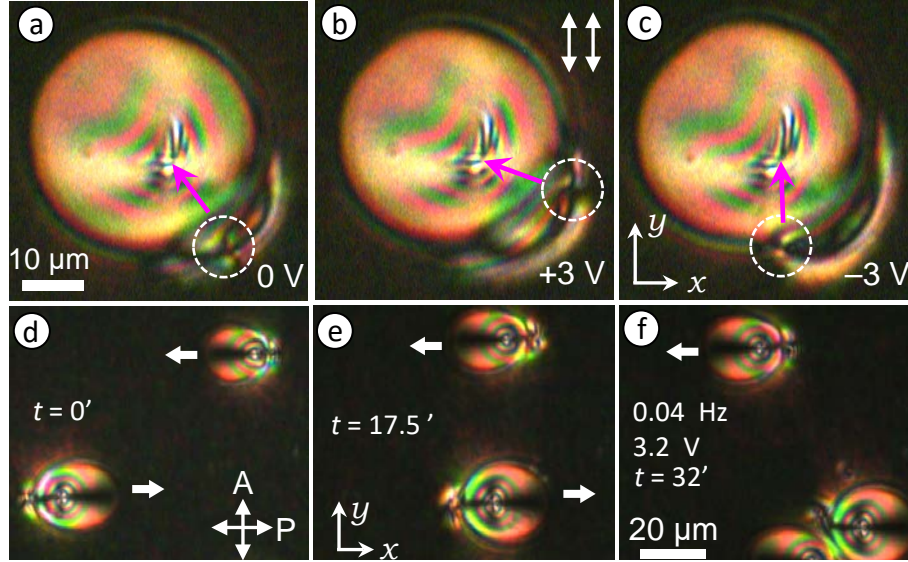


Figure 22. (a-c) N- N_{TB} biphasic state of C-HB3 (i.e., SBCN1 with 3 wt % HB) in a 90°-twist cell with alignments along x and y at top and bottom, respectively.; the dark background is of N matrix in which is seen a large birefringent N_{TB} drop coupled to the encircled satellite -1 defect created in the nematic. In the field-free state (a), the dipole is diagonally oriented along the midplane director relative to x . In top view, for positive voltages, the -1 defect appears to navigate around the drop toward the x -axis by the shortest path; for negative voltages, by contrast, the defect seems to glide toward the y -axis. The angular displacement increases nonlinearly with U . (d-e) Select frames of a time series showing oppositely drifting dipoles in a 20 μm thick planar layer of C-OP3 (i.e., SBCN1 with 3 wt % OP) subjected to a sine wave field of frequency 0.04 Hz and rms voltage 3.2 V. Dark background is of nematic medium aligned along x . In (c), the lower of the two dipoles is coupled antiparallely to the one attracted to it from below. (After [60]).

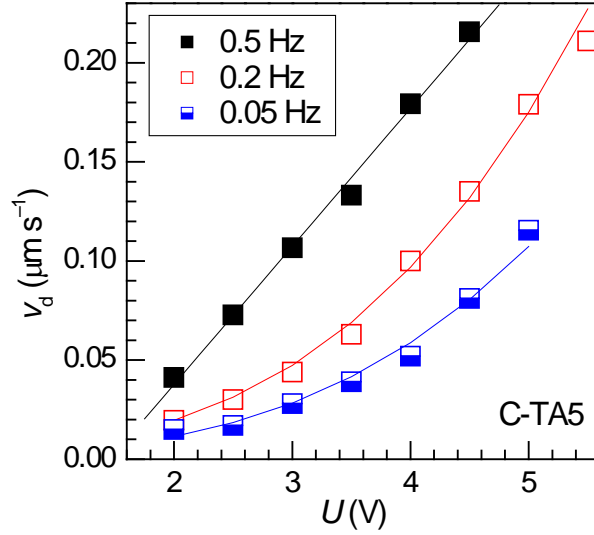


Figure 23. Drift velocity of dipoles as a function of applied voltage at different frequencies in a 20 μm thick layer of C-TA5 (i.e., SBCN1 with 5 wt % TA); planar cell at 91.3 $^{\circ}\text{C}$. The continuous line for 0.5 Hz is a linear fit; the lines for 0.05 Hz and 0.2 Hz are according to $v_d = aU + bU^3$. (After [60]).

4.4. Topological defects and surrounding periodic patterns in BCNs

Kumar et al. [72, 73] have studied various electric field effects pertaining to generation of topological defects and periodic patterns in the bent-rod nematic DBCN4. An initially homeotropic nematic layer of DBCN4, upon excitation by ac fields of frequency well above the dielectric inversion point f_i , shows several structural transitions; see the phase diagram in Figure 24(a). The compound, which belongs to the $(- +)$ class beyond f_i , bifurcates first into the bend Freedericksz (BF) state at U_F ; periodic instabilities follow as secondary bifurcations. Well above U_F , an anchoring transition takes place from the BF state to the degenerate planar (DP) state that persists for several hours even after the field is switched off. At the onset of BF distortion, numerous $+1$ and -1 umbilics form, the former being mostly of the chiral type. They remain in the DP state as nonsingular disclinations. In the BF regime, close to f_i , radial domains similar to NRs of s-EC form around $+1$ umbilics above U_{EC} ; they propagate along the local wave vector right from

their onset. With increasing f , the wave vector switches from tangential to radial disposition [Figure 24 (b)-(e)]. Far above f_i , a broad-band instability that resembles the prewavy instability is found. In the DP state, normal rolls, broad domains, and chevrons (both defect-mediated and defect-free types [133]) form around various line defects, in different regions of the f - U plane. A significant feature common to *all* the different patterned states is the travelling wave phenomenon [Figure 25]. Intriguingly, this feature is *not* observed with well aligned planar layers of DBCN4. It is, therefore, possible that line defects with broken symmetry play an important role in causing the propagative instability.

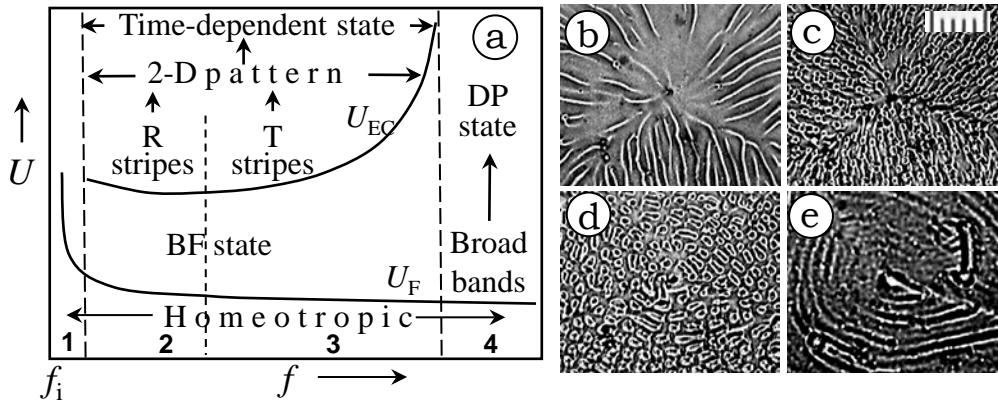


Figure 24. (a) Schematic of the bifurcation states in the voltage-frequency space inside the conduction regime, above the dielectric isotropy point f_i for DBCN4. U_F and U_{EC} denote the critical voltages for the onset of bend-Freedericksz (BF) and electroconvective (EC) instabilities, respectively. The BF and EC states in regions 2 and 3 are metastable and give way to the degenerate planar (DP) state or a patterned state arising out of it. In region 4, the BF state is unstable to the formation of broad bands. (b-e) Sequence of transformation from the tangential to radial wave vector state (i.e., R stripes \rightarrow T stripes) under increasing frequency and constant voltage (20 V). Natural light; $f = 190$ kHz (b), 210 kHz (c), 230 kHz (d) and 260 kHz (e). $d = 18.6 \mu\text{m}$. 140°C . Scale division $10 \mu\text{m}$. (After [72, 73]).

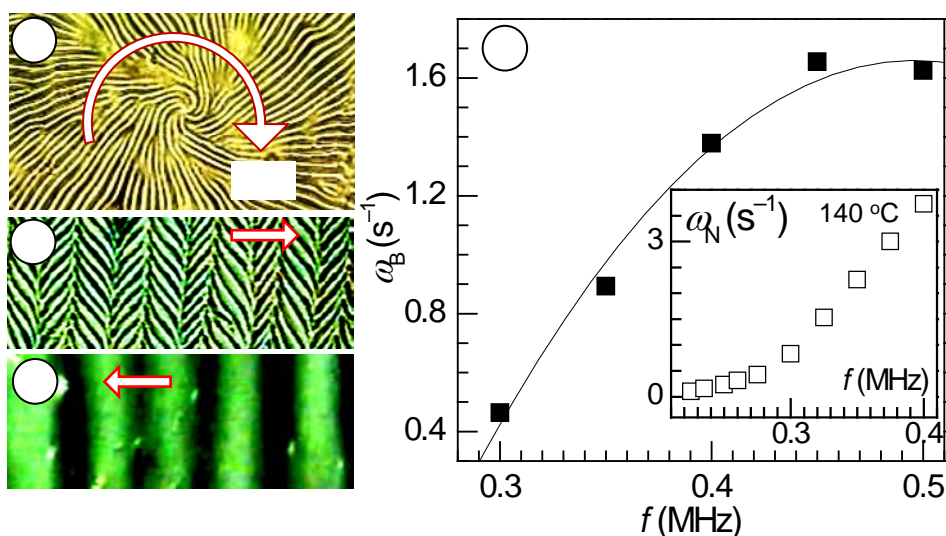


Figure 25. Phase propagation in different patterned states of DBCN4. (a) NRs around a +1 defect (490 kHz, 23.5 V, 140 °C, $d = 19.3 \mu\text{m}$), (b) DMCs (200 kHz, 17 V, 135 °C, $d = 14.7 \mu\text{m}$), (c) BDs (300 kHz, $V = 28.1 \text{ V}$, 138 °C, $d = 14.7 \mu\text{m}$). (d) Propagation frequency $\omega_B = q v_d$ (q being the wave number and v_d the drift speed) as a function of f for broad domains near threshold voltage; inset: Propagation frequency ω_N of NRs as a function of f , near threshold. Threshold voltages U_c are: $-8.1 + 115 f$ (MHz) for BDs, and $15.6 - 136 f$ (MHz) + $494 f^2$ for NRs. (After [72, 73]).

5. Closing remarks

In closing, it will be useful to indicate the areas of concern requiring future work on the subject of this review. Though the range of usable BCN compounds is limited and the understanding of electrically generated structures in them is far from complete, it is clear that the richness of distinctive electrical phenomena in BCNs is no less than in calamitics. Speaking particularly of patterned states in calamitics, despite a long history of their investigation, there still remain some intriguing questions over the origin of nonstandard features of EC. In view of this, it is unsurprising that some scenarios of BCN patterns, like ‘banana-specificity’, still await an explanation.

The nanostructures of BCNs are known to substantially differ from those of calamitics. This is perhaps the reason for several material properties of BCNs falling relatively into a different parameter range. It is, however, yet unclear as to how these differences could lead to the observed specific features. A more detailed exploration of material parameters and pattern characteristics, together with extended numerical simulations based on known theoretical models and BCN properties might be required to clarify the various issues. Pattern formation in the N_{TB} phase, which is mostly an unexplored phenomenon having no analogy in calamitic nematics, also invites further studies.

Though BCNs are not expected to affect the LC display market, the patterns reviewed may open up new horizons for developing photonic devices. Pattern formation in chiral BCNs (which did not belong to the scope of the present review) may offer further possibilities in this field.

Coming to the work on electrically generated point-, line- and wall defects in the three categories of BCNs, clearly an impressive variety of new structures have been reported. Here again there are fundamental questions relating to the underlying physics that need further attention. For example, the inplane vortices of flow in the PW instability (so different from the vortices of s-EC due to coulombic forces on space charges) and the corresponding coherent inplane motion of disclinations in the ILR and INR convection states at elevated constraints are nonlinear effects that are still to find a theoretical description. Similarly, it would be useful to have numerical simulations of translation of elastic dipoles due to hybrid flexoelectric-dielectric backflows in nematic colloids, with N_{TB} drops as the dispersed phase. Finally, N_{TB} drops in the biphasic $N-N_{TB}$ region are known to grow through a systematic development of internal defects [134]. While we have not reviewed these defects because of their formation even

without any electric field, their nucleation and growth, leading to complex drop-geometries, are known to be facilitated by electric fields. The uncommon shape of such N_{TB} drops and the structure of their internal defects are areas attractive for future experimental and theoretical advances.

References

- [1] Takezoe H, Takanishi Y. Bent-core liquid crystals: Their mysterious and attractive world. *Jpn. J. Appl. Phys.* 2006;45:597–625.
- [2] Yu FC, Yu L. J. Mesophases of achiral bent molecules. *Chem. Mater.* 2006;18:5410–5420.
- [3] Jáklí A, Lavrentovich OD, Selinger JV. Physics of liquid crystals of bent-shaped molecules. *Rev. Mod. Phys.* 2018;90:045004.
- [4] Niori T, Sekine T, Watanabe J, et al. Distinct ferroelectric smectic liquid crystals consisting of banana shaped achiral molecules. *J. Mater. Chem.* 1996;6:1231–1233.
- [5] Jáklí A. Liquid crystals of the twenty-first century – Nematic phase of bent-core molecules. *Liq. Cryst. Rev.* 2013;1:65–82.
- [6] Gleeson HF, Kaur S, Görtz V, et al. The nematic phases of bent-core liquid crystals. *ChemPhysChem* 2014;15:1251–1260.
- [7] Vita F, Adamo FC, Francescangeli O. Polar order in bent-core nematics: An overview. *J. Mol. Liq.* 2018;267:564–573.
- [8] Bailey CA, Fodor-Csorba K, Gleeson JT, et al. Rheological properties of bent-core liquid crystals. *Soft Matter* 2009;5:3618.
- [9] Sathyanarayana P, Mathew M, Li Q, et al. Splay bend elasticity of a bent-core nematic liquid crystal. *Phys. Rev. E* 2010;81:010702(R).
- [10] Majumdar M, Salamon P, Jáklí A, et al. Elastic constants and orientational viscosities of a bent-core nematic liquid crystal. *Phys Rev E* 2011;83:031701.
- [11] Sathyanarayana P, Jampani VSR, Skarabot M, et al. Viscoelasticity of ambient-temperature nematic binary mixtures of bent-core and rodlike molecules. *Phys. Rev. E* 2012;85:011702.

- [12] Salamon P, Éber N, Buka Á, et al. Dielectric properties of mixtures of a bent-core and a calamitic liquid crystal. *Phys. Rev. E* 2010;81:031711.
- [13] Tadapatri P, Krishnamurthy KS, Weissflog W. Multiple electroconvection scenarios in a bent-core nematic liquid crystal. *Phys. Rev. E* 2010;82:31706.
- [14] Harden J, Mbanga B, Éber N, et al. Giant flexoelectricity of bent-core nematic liquid crystals. *Phys. Rev. Lett.* 2006;97:157802.
- [15] Stojadinovic S, Adorjan A, Sprunt SN, et al. Dynamics of the nematic phase of a bent-core liquid crystal. *Phys. Rev. E* 2002;66:060701(R).
- [16] Domenici V, Veracini CA, and Zalar B. How do banana-shaped molecules get oriented (if they do) in the magnetic field?. *Soft Matter* 2005;1:408–411.
- [17] Chakraborty S, Gleeson JT, Jákli A, et al. A comparison of short-range molecular order in bent-core and rod-like nematic liquid crystals. *Soft Matter* 2013;9:1817–1824.
- [18] Hong SH, Verduzco R, Gleeson JT, et al. Nanostructures of liquid crystal phases in mixtures of bent-core and rod-shaped molecules. *Phys. Rev. E* 2011;83:061702.
- [19] Zhang C, Gao M, Diorio NJ, et al. Direct observation of smectic layers in thermotropic liquid crystals. *Phys. Rev. Lett.* 2012;109:107802.
- [20] Freiser MJ. Ordered states of a nematic liquid. *Phys. Rev. Lett.* 1970;24: 1041–1043.
- [21] Yu LJ, Saupe A. Observation of a biaxial nematic phase in potassium laurate-1-decanol-water mixtures. *Phys. Rev. Lett.* 1980;45:1000–1004.
- [22] Dozov I. On the spontaneous symmetry breaking in the mesophases of achiral banana-shaped molecules. *Europhys. Lett.* 2001;56:247–253.
- [23] Borshch V, Kim YK, Xiang J, et al. Nematic twist-bend phase with nanoscale modulation of molecular orientation. *Nat. Commun.* 2013;4:2635
- [24] Chen D, Porada JH, Hooper JB, et al. Chiral heliconical ground state of nanoscale pitch in a nematic liquid crystal of achiral molecular dimers. *Proc. Natl. Acad. Sci. U.S.A.* 2013;110:15931–15936.
- [25] Wiant DB, Gleeson JT, Éber N, et al. Non-standard electroconvection in a bent core nematic. *Phys. Rev. E* 2005;72:041712.
- [26] Jákli A, Chambers M, Harden J, et al. Extraordinary properties of nematic phases of bent-core liquid crystals. In: *Proceedings of Emerging Liquid Crystal Technologies III*, San Jose, January 20-24, 2008, *Proc. SPIE* 2008;6911:691105.

- [27] Le KV, Araoka F, Fodor-Csorba K, et al. Flexoelectric effect in a bent-core mesogen. *Liquid Crystals* 2009;36:1119–1124.
- [28] Tanaka S, Takezoe H, Éber N, et al. Electroconvection in nematic mixtures of bent-core and calamitic molecules. *Phys. Rev. E* 2009;80:021702.
- [29] Buka Á, Éber N, Fodor-Csorba K, et al. Physical properties of a bent-core nematic liquid crystal and its mixtures with calamitic molecules. *Phase Transitions* 2012;85:872–887.
- [30] Elamain O, Hegde G, Komitov L. Polar flexoelectric in-plane and out-of-plane switching in bent core nematic mixtures. *Jpn. J. Appl. Phys.* 2016;55:71701.
- [31] Weissflog W, Sokolowski S, Dehne H, et al. Chiral ordering in the nematic and an optically isotropic mesophase of bent-core mesogens with a halogen substituent at the central core. *Liquid Crystals* 2004;31:923–933.
- [32] Elamain O, Hegde G, Komitov L. Periodic pattern formation in an achiral bent core nematic. *AIP Advances* 2018;8:095227.
- [33] Tadapatri P, Krishnamurthy KS, Weissflog W. Patterned flexoelectric instability in a bent-core nematic liquid crystal. *Soft Matter* 2012;8:1202–1214.
- [34] Tadapatri P, Krishnamurthy KS. Competing instability modes in an electrically driven bent-core nematic liquid crystal. *J. Phys. Chem. B* 2012;116:782–793.
- [35] Krishnamurthy KS. Spatiotemporal character of the Bobylev-Pikin flexoelectric instability in a twisted nematic bent-core liquid crystal exposed to very low frequency fields. *Phys. Rev. E* 2014;89:052508.
- [36] Pelzl G, Eremin A, Diele S, et al. Spontaneous chiral ordering in the nematic phase of an achiral banana-shaped compound. *J. Mater. Chem.* 2002;12:2591–2593.
- [37] Krishnamurthy KS, Tadapatri P, Weissflog W. Twist disclination loops in a bent-core nematic liquid crystal. *Soft Matter* 2011;7:6273–6284.
- [38] Kovalenko L, Schröder MW, Amaranatha Reddy R, et al. Unusual mesomorphic behaviour of new bent-core mesogens derived from 4-cyanoresorcinol. *Liquid Crystals* 2005;32:857–865.
- [39] Krishnamurthy KS, Tadapatri P, Viswanath, P. Dislocations and metastable chevrons in the electroconvective inplane normal roll state of a bent core nematic liquid crystal. *Soft Matter* 2014;10:7316–7327.
- [40] Tadapatri P, Hiramath US, Yelamaggad CV, et al. Patterned electroconvective states in a bent-core nematic liquid crystal. *J. Phys. Chem. B* 2010;114:10–21.

- [41] Tanaka S, Dhara S, Sadashiva BK, et al., Alternating twist structures formed by electroconvection in the nematic phase of an achiral bent-core molecule. *Phys. Rev. E* 2008;77:041708.
- [42] Xiang Y, Goodby JW, Görtz V, et al. Revealing the uniaxial to biaxial nematic liquid crystal phase transition via distinctive electroconvection. *Appl. Phys. Lett.* 2009;94:193507.
- [43] Kaur S, Belaisaoui A, Goodby JW, et al. Nonstandard electroconvection in a bent-core oxadiazole material. *Phys. Rev. E* 2011;83:041704.
- [44] Kaur S, Panov VP, Greco C, et al. Flexoelectricity in an oxadiazole bent-core nematic liquid crystal. *Appl. Phys. Lett.* 2014;105:223505.
- [45] Xu M, Zhou M, Xiang Y, et al. Domain structures as optical gratings controlled by electric field in a bent-core nematic. *Optics Express* 2015;23:15224.
- [46] Yuan R, Feng H, Xing H-y, et al. Flexodomain in BCN liquid crystal. *Chin. J. Liq. Cryst. Disp.* 2016;31:870–876.
- [47] Xiang Y, Jing H, Zhang Z, et al. Tunable optical grating based on the flexoelectric effect in a bent-core nematic liquid crystal. *Phys. Rev. Appl.* 2017;7:064032.
- [48] Éber N, Xiang Y, Buka Á. Bent core nematics as optical gratings. *J. Mol. Liq.* 2018;267:436–444.
- [49] Pesch W, Krekhov A, Éber N., et al., Nonlinear analysis of flexodomains in nematic liquid crystals. *Phys. Rev. E* 2018;98:032702.
- [50] Yuan R., Ye W-J, Xing H-Y, et al. Continuously adjustable period optical grating based on flexoelectric effect of a bent-core nematic liquid crystal in planar cells. *Optics Express* 2018;26:4288–4299.
- [51] Xiang Y, Liu Y, Buka Á, et al. Electric-field-induced patterns and their temperature dependence in a bent-core liquid crystal. *Phys. Rev. E* 2014;89:012502.
- [52] Xiang Y, Zhou M, Xu M, et al. Unusual polarity-dependent patterns in a bent-core nematic liquid crystal under low-frequency ac field. *Phys. Rev. E* 2015;91:042501.
- [53] Jing H, Xu M, Xiang Y, et al. Light tunable gratings based on flexoelectric effect in photoresponsive bent-core nematics. *Adv. Optical Mater.* 2019;7:1801790.
- [54] Le KV, Mathews M, Chambers M, et al. Electro-optic technique to study biaxiality of liquid crystals with positive dielectric anisotropy: The case of a bent-core material. *Phys. Rev. E* 2009;79:030701(R).

- [55] Krishnamurthy KS, Palakurthy NB, Yelamaggad CV. Confined electroconvective and flexoelectric instabilities deep in the Freedericksz state of nematic CB7CB. *J. Phys. Chem. B* 2017;121:5447.
- [56] Krishnamurthy KS, Kanakala MB, Yelamaggad CV, et al. Instabilities in the electric Freedericksz state of the twist-bend nematic liquid crystal CB7CB. *Soft Matter* 2018;14:5393.
- [57] Kleman M, Krishnamurthy KS. Defects in the twist-bend nematic phase: Stabilities and instabilities of focal conic domains and related topics. *Phys. Rev. E* 2018;98:032705.
- [58] Vaupotič N, Ali M, Majewski PW, et al. *Chem. Phys. Chem.* 2018;19:2566–2571.
- [59] Lin Y-C, Wu P-C, Lee W. Frequency-modulated textural formation and optical properties of a binary rod-like/bent-core cholesteric liquid crystal. *Photonics Research* 2019;7:1258–1265.
- [60] Krishnamurthy KS, Shankar Rao DS, Kanakala MB, et al. Electric response of topological dipoles in nematic colloids with twist-bend nematic droplets as the dispersed phase. *Phys. Rev. E.* 2021;103:042701.
- [61] Panov VP, Nagaraj M, Vij JK, et al. Spontaneous periodic deformations in nonchiral planar-aligned bimesogens with a nematic-nematic transition and a negative elastic constant. *Phys. Rev. Lett.* 2010;105:167801.
- [62] Panov VP, Vij JK, Balachandran R, et al. Properties of the self-deforming N_{tb} phase in mesogenic dimers. In *Liquid Crystals XVII*, edited Khoo IC, Proc. SPIE 2013;8828:88280X.
- [63] Mandle RJ, Davis EJ, Archbold CT, et al. Microscopy studies of the nematic NTB phase of 1,11-di-(100-cyanobiphenyl-4-yl)undecane. *J. Mater. Chem. C* 2014;2:556–566.
- [64] You R, Paterson DA, Storey JMD, et al. Formation of periodic zigzag patterns in the twist-bend nematic liquid crystal phase by surface treatment. *Liquid Crystals* 2017;44:168–176.
- [65] Panov VP, Balachandran R, Nagaraj M, et al. Microsecond linear optical response in the unusual nematic phase of achiral bimesogens. *Appl. Phys. Lett.* 2011;99:261903.
- [66] Panov VP, Balachandran R, Vij JK, et al. Field-induced periodic chiral pattern in the N_x phase of achiral bimesogens. *Appl. Phys. Lett.* 2012;101:234106.

- [67] Tamba MG, Kosata B, Pelz K, et al. Mesogenic dimers composed of a calamitic and a bent-core mesogenic unit. *Soft Matter* 2006;2:60–65.
- [68] Tamba M-G, Weissflog W, Eremin A, et al. Electro-optic characterization of a nematic phase formed by bent core mesogens. *Eur. Phys. J. E* 2007;22:85–95.
- [69] Stannarius R, Eremin A, Tamba M-G, et al. Field-induced texture transitions in a bent-core nematic liquid crystal. *Phys. Rev. E* 2007;76:061704.
- [70] Stannarius R, Heuer J. Electroconvection in nematics above the splay Fréedericksz transition. *Eur. Phys. J. E* 2007;24:27–33.
- [71] Heuer J, Stannarius R, Tamba M-G, et al. Longitudinal and normal electroconvection rolls in a nematic liquid crystal with positive dielectric and negative conductivity anisotropy. *Phys. Rev. E* 2008;77:056206.
- [72] Kumar P, Hiremath US, Yelamagad CV, et al. Electroconvection in a homeotropic bent-rod nematic liquid crystal beyond the dielectric inversion frequency. *J. Phys. Chem. B* 2008;112:9753–9760.
- [73] Kumar P, Hiremath US, Yelamagad CV, et al. Drifting periodic structures in a degenerate-planar bent-rod nematic liquid crystal beyond the dielectric inversion frequency. *J. Phys. Chem. B* 2008;112:L9270.
- [74] Éber N, Salamon P, Buka Á. Electrically induced patterns in nematics and how to avoid them. *Liquid Crystals Reviews* 2016;4:101–134.
- [75] Buka Á, Éber N, Pesch W, et al. Convective patterns in liquid crystals driven by electric field. In: Golovin AA, Nepomnyashchy AA, editors. *Self-Assembly, Pattern Formation and Growth Phenomena in Nano-Systems*. Dordrecht: Springer; 2006. (NATO Science Series II, Mathematica, Physics and Chemistry, Vol. 218).
- [76] Bodenschatz E, Zimmermann W, Kramer L. On electrically driven patternforming instabilities in planar nematics. *J. Phys. (Paris)* 1988;49:1875–1899.
- [77] Huh J-H, Hidaka Y, Yusril Y, et al. Prewavy pattern: a director-modulation structure in nematic liquid crystals. *Mol. Cryst. Liq. Cryst.* 2001;364:111–122.
- [78] Krekhov A, Pesch W, Buka Á. Flexoelectricity and pattern formation in nematic liquid crystals. *Phys. Rev. E* 2011;83:051706.
- [79] Panov VP, Varney MCM, Smalyukh I, et al. Hierarchy of periodic patterns in the twist-bend nematic phase of mesogenic dimers. *Mol. Cryst. Liq. Cryst.* 2015;611:180–185.

- [80] Challa PK, Borshch V, Parri O, et al. Twist-bend nematic liquid crystals in high magnetic fields. *Phys. Rev. E* 2014;89:060501(R).
- [81] de Almeida RRR, Zhang C, Parri O, et al. Nanostructure and dielectric properties of a twist-bend nematic liquid crystal mixture. *Liq. Cryst.* 2014;41:1661–1667.
- [82] Sreenilayam SP, Panov VP, Vij JK et al. The N_{TB} phase in an achiral asymmetrical bent-core liquid crystal terminated with symmetric alkyl chains. *Liq. Cryst.* 2017;44:244–253.
- [83] Jákli A. Private communication.
- [84] Elamain O, Hegde G, Fodor-Csorba K, et al. Field-induced optically isotropic state in bent core nematic liquid crystals: unambiguous proof of field-induced optical biaxiality. *J. Phys. D: Appl. Phys.* 2013;46:455101.
- [85] Krishnamurthy KS, Kumar P, Kumar MV. Polarity-sensitive transient patterned state in a twisted nematic liquid crystal driven by very low frequency fields, *Phys. Rev. E* 2013;87:022504.
- [86] Dennin M, Ahlers G, Cannell DS. Chaotic localized states near the onset of electroconvection. *Phys. Rev. Lett.* 1996;77:2475–2478.
- [87] Kumar P, Krishnamurthy KS. Competing modes of instability in an electrically driven nematic liquid crystal with a small positive dielectric anisotropy. *Phys. Rev. E* 2006;74:031705.
- [88] Vistin' LK. Electrostructural effect and optical properties of a certain class of liquid crystals and their binary mixtures, *Sov. Phys. Crystallogr.* 1970;15:514 [Kristallografiya 1970;15:594 (in Russian)].
- [89] Vistin' LK. New electrostructural effect in liquid crystals of nematic type, *Sov. Phys. Dokl.* 1971;15:908 [Dokl. Akad. Nauk SSSR 1970;194:1318 (in Russian)].
- [90] Barnik MI, Blinov LM, Trufanov AN, et al. Flexoelectric domains in nematic liquid crystals, *Sov. Phys. JETP* 1977;46:1016 [Zh. Eksp. Teor. Fiz. 1977;73:1936 (in Russian)].
- [91] Barnik MI, Blinov LM, Trufanov AN, et al. Flexo-electric domains in liquid crystals, *J. Phys. (France)* 1978;39:417.
- [92] Bobylev YuP, Pikin SA. Threshold piezoelectric instability in a liquid crystal, *Sov. Phys. JETP* 1977;45:195 [Zh. Eksp. Teor. Fiz. 1977;72:369 (in Russian)].
- [93] Buka Á, Éber N, editors. *Flexoelectricity in Liquid Crystals. Theory, Experiments and Applications*, London: Imperial College Press; 2012.

- [94] Jákli A, Harden J, Éber N. Chapter 3. Flexoelectricity of bent-core molecules, In: Buka Á, Éber N, editors. Flexoelectricity in Liquid Crystals. Theory, Experiments and Applications. London: Imperial College Press; 2012. pp. 61–99.
- [95] Madhusudana NV. Chapter 2. Flexoelectro-optics and measurements of flexocoefficients, In: Buka Á, Éber N, editors. Flexoelectricity in Liquid Crystals. Theory, Experiments and Applications. London: Imperial College Press; 2012. pp. 33–60.
- [96] Ferrarini A, Greco C, Luckhurst GR. On the flexoelectric coefficients of liquid crystal monomers and dimers: a computational methodology bridging length-scales. *J. Mater. Chem.* 2007;17:1039–1042.
- [97] Kundu B, Roy A, Pratibha R, et al. Flexoelectric studies on mixtures of compounds made of rodlike and bent-core molecules. *Appl. Phys. Lett.* 2009;95:81902.
- [98] Kumar P, Marinov YG, Hinov HP, et al. Converse flexoelectric effect in bent-core nematic liquid crystals. *J. Phys. Chem. B* 2009;113:9168.
- [99] Cestari M, Frezza E, Ferrarini A, et al. Crucial role of molecular curvature for the bend elastic and flexoelectric properties of liquid crystals: mesogenic dimers as a case study. *J. Mater. Chem.* 2011;21:12303–12308.
- [100] Lee J-H, Yoon T-H, Choi E-J. Flexoelectric effect of a rod-like nematic liquid crystal doped with highly-kinked bent-core molecules for energy converting components. *Soft Matter* 2012;8:2370–2374.
- [101] Sathyanarayana P, Dhara S. Antagonistic flexoelectric response in liquid crystal mixtures of bent-core and rodlike molecules. *Phys. Rev. E* 2013;87:12506.
- [102] Sreenilayam SP, Panarin YuP, Vij JK, et al. Flexoelectric polarization studies in bent-core nematic liquid crystals. *Phys. Rev. E* 2015;92:022502.
- [103] Lee D-J, Choi J-C, Park M-K, et al. Optical measurement of flexoelectric polarization change in liquid crystals doped with bent-core molecules using hybrid-aligned structure. *Liquid Crystals* 2017;44:1321–1331.
- [104] Rudquist P, Lagerwall ST. Chapter 7. Applications of Flexoelectricity, In: Buka Á, Éber N, editors. Flexoelectricity in Liquid Crystals. Theory, Experiments and Applications. London: Imperial College Press; 2012. pp. 211–247.
- [105] Blatch AE, Coles MJ, Musgrave BB, et al. Flexoelectric liquid crystal bimesogens. *Mol. Cryst. Liq. Cryst.* 2003;401:47–55.

- [106] Coles HJ, Clarke MJ, Morris SM, et al. Strong flexoelectric behavior in bimesogenic liquid crystals. *J. Appl. Phys.* 2006;99:34104.
- [107] Aziz N, Kelly SM, Duffy W, et al. Banana-shaped dopants for flexoelectric nematic mixtures. *Liquid Crystals* 2008;35:1279–1292.
- [108] Salter PS, Tschierske C, Elston SJ, et al. Flexoelectric measurements of a bent-core nematic liquid crystal. *Phys. Rev. E* 2011;84:031708.
- [109] Atkinson KL, Morris SM, Castles F, et al. Flexoelectric and elastic coefficients of odd and even homologous bimesogens. *Phys. Rev. E* 2012;85:11701.
- [110] Atkinson KL, Morris SM, Qasim MM, et al. Increasing the flexoelastic ratio of liquid crystals using highly fluorinated ester-linked bimesogens. *Phys. Chem. Chem. Phys.* 2012;14:16377–16385.
- [111] Balachandran R, Panov VP, Vij JK, et al. Effect of cybotactic clusters on the elastic and flexoelectric properties of bent-core liquid crystals belonging to the same homologous series. *Phys. Rev. E* 2013;88:32503.
- [112] Balachandran R, Panov VP, Panarin YuP, et al. Flexoelectric behavior of a bimesogenic liquid crystal. *Mol. Cryst. Liq. Cryst.* 2015;611:65–70.
- [113] Varanytsia A, Chien L-C. Bimesogen-enhanced flexoelectro-optic behavior of polymer stabilized cholesteric liquid crystal. *J. Appl. Phys.* 2016;119:014502.
- [114] Meyer C, Luckhurst GR, Dozov I. Flexoelectrically driven electroclinic effect in the twist-bend nematic phase of achiral molecules with bent shapes. *Phys. Rev. Lett.* 2013;111:067801.
- [115] Varanytsia A, Chien L-C. Giant flexoelectro-optic effect with liquid crystal dimer CB7CB. *Sci. Reports* 2017;7:41333. |
- [116] Castles F, Morris SM, Coles HJ. The limits of flexoelectricity in liquid crystals. *AIP Advances* 2011;1:32120. *Sci. Reports* 2017;7:41333.
- [117] Palffy-Muhoray P. Comment on “The limits of flexoelectricity in liquid crystals” [*AIP Advances*1, 032120 (2011)]. *AIP Advances* 2013;3:019101.
- [118] Castles F, Morris SM, Coles HJ. Response to “Comment on ‘The limits of flexoelectricity in liquid crystals’” [*AIP Advances*3, 019101 (2013)]. *AIP Advances* 2013;3:19102.
- [119] Harden J, Teeling R, Gleeson JT, et al. Converse flexoelectric effect in a bent-core nematic liquid crystal. *Phys. Rev. E* 2008;78:031702.
- [120] Salamon P. Private communication.

- [121] Morris R, Jones JC, Nagaraj M. Variable pitch hydrodynamic electro-optic gratings utilising bent liquid crystal dimers. *Soft Matter* 2020;16:10439.
- [122] Xiang Y, Jing H, Sun W, et al. Topological defects arrays and control of electro-convections in periodically photo-aligned bent-core nematics. *J. Mol. Liq.* 2020;318:114058.
- [123] Krishnamurthy KS, Kanakala MB, Yelamaggad CV, et al. Microscale structures arising from nanoscale inhomogeneities in nematics made of bent-shaped molecules. *J. Phys. Chem. B* 2019;123:1423–1431.
- [124] Kleman M, Lavrentovich OD. Topological point defects in nematic liquid crystals. *Phil. Mag.* 2006;86:4117–4137.
- [125] Muševič I. *Liquid Crystal Colloids*. Cham, Switzerland: Springer;2017.
- [126] Stark H. Physics of colloidal dispersions in nematic liquid crystals. *Phys. Rep.* 2001;351:387–474.
- [127] De Gennes, PG, Prost J. *The Physics of Liquid Crystals*, 2nd Edn. Oxford: Oxford University Press; 1993.
- [128] Goren G, Procaccia I, Rasenat S, et al. Interactions and dynamics of topological defects: Theory and experiments near the onset of weak turbulence. *Phys. Rev. Lett.* 1989;63:1237–1240.
- [129] Rasenat S, Steinberg V, Rehberg I. Experimental studies of defect dynamics and interaction in electrohydrodynamic convection. *Phys. Rev. A* 1990;42:5998–6008.
- [130] Joets A, Ribotta R. Hydrodynamic transitions to chaos in the convection of an anisotropic fluid. *J. Phys. (Paris)* 1986;47:595–606.
- [131] Friedel J, De Gennes PG. Boucles de disclination dans les cristaux liquides. [Disclination loops in liquid crystals]. *C.R. Acad. Sc. Paris B* 1969;268:257–259. In French.
- [132] Sonnet AM, Virga EG. Dynamics of nematic loop disclinations. *Phys. Rev. E* 1997; 56:6834–6842.
- [133] Huh J-H, Hidaka Y, Rossberg AG, et al. Pattern formation of chevrons in the conduction regime in homeotropically aligned liquid crystals. *Phys. Rev. E* 2000;61:2769–2776.
- [134] Krishnamurthy KS, Shankar Rao DS, Kanakala MB, et al. Topological defects due to twist-bend nematic drops mimicking colloidal particles in a nematic medium. *Soft Matter* 2020;16:7479–7491.